Article

Water Dynamics and Morphometric Parameters of Lake Sevan (Armenia) in the Summer–Autumn Period According to Satellite Data

Anna I. Ginzburg [1], Andrey G. Kostianoy [1,2,3,*], Nickolay A. Sheremet [1] and Olga Yu. Lavrova [4]

[1] Shirshov Institute of Oceanology, Russian Academy of Sciences, 36, Nakhimovsky Pr., Moscow 117997, Russia; ginzburg@ocean.ru (A.I.G.); sheremet@ocean.ru (N.A.S.)
[2] Laboratory of Integrated Research of Water Resources, S.Yu. Witte Moscow University, 12, Build 1, Second Kozhukhovsky Proezd, Moscow 115432, Russia
[3] Laboratory of Geoinformatics, Geoecology and Rational Environmental Management, Faculty of Engineering, Maykop State Technological University, 191, Pervomayskaya Str., Maykop 385000, Russia
[4] Space Research Institute, Russian Academy of Sciences, 84/32, Profsoyuznaya Str., Moscow 117997, Russia; olavrova@iki.rssi.ru
[*] Correspondence: kostianoy@ocean.ru

Abstract: Here, we explore the dynamics of the waters of eutrophicated Lake Sevan in the modern period, using MSI Sentinel-2 satellite images of different months in different years (2017–2022) and SAR Sentinel-1 images of similar dates. The main objective of the study is to investigate the spatiotemporal variability of the horizontal circulation of this lake and to establish whether the scheme of cyclonic water circulation in the deep-water part of Large Sevan, given in a number of publications, which does not imply water exchange between its littoral and deep-water zones, corresponds to the real picture of currents in the surface layer of the lake in the summer–autumn period (period of pronounced water stratification and intense phytoplankton bloom). The analysis performed convincingly showed that there is no constant cyclonic gyre on the scale of the deep-water part of Large Sevan ($\approx$20 km) during the period under consideration. In most cases, non-stationary eddy dynamics are observed in Large Sevan, including mesoscale and submesoscale eddies, eddy dipoles (mushroom-shaped flows), and their packings. Often the entire deep-water part of Large Sevan is occupied by a two-cell (dipole) or even three-cell (cyclonic eddy with two anticyclones of similar size) water circulation. The time scale of the observed variability is several days. Such variable water circulation in different months (i.e., with different density stratification of water) of different years in a basin with a fairly homogeneous bottom and a slight indentation of the shoreline raises the assumption that the main reason for the non-stationary dynamics in Large Sevan is the variability of the wind effect on its surface layer. The cyclonic gyre in Small Sevan (8–9 km) is a permanent element of the circulation and maintains its position north of the strait between Small and Large Sevan. This gyre and attached anticyclonic eddies in the southern part of its periphery, as well as cyclonic submesoscale eddies in the northern part of Large Sevan, close to the strait, affect the water exchange between Small and Large Sevan in both directions. An additional objective of the study is a validation of the morphometric parameters of Lake Sevan (level, surface area, and water volume), contained in the near-real time HYDROWEB database, LEGOS, France (June 1995–January 2024), based on their comparison with the corresponding values of these parameters from gauging stations in Armenia. It is shown that, with a qualitative correspondence of the nature of lake level changes according to altimetric and instrumental measurements, its values in the HYDROWEB database exceed the data of gauging stations in most cases by 1–1.5 m in 1995–2012 and 0.5–0.6 m in 2013–2022, while the corresponding surface area and volume values according to HYDROWEB data turn out to be underestimated.

Keywords: Lake Sevan; lake eutrophication; algal bloom; remote sensing; horizontal water circulation; eddies; eddy dipoles; MSI Sentinel-2 imagery; SAR Sentinel-1 images; morphometric parameters; HYDROWEB database

1. Introduction

Lake Sevan, located on the territory of Armenia ($40°09'$–$40°38'$N, $44°57'$–$45°39'$E) at an altitude of approximately 1900 m above sea level and surrounded by mountain ranges up to 3600–3800 m high (up to 1900 m above lake level) is one of the largest alpine freshwater lakes in the world [1–3] and the second highest freshwater lake after Lake Titicaca in South America [1,4]. Lake Sevan is of great importance for fishing, agriculture, livestock farming, industry, and recreation and tourism of the Republic of Armenia, as well as a repository of its strategic freshwater reserves.

The lake consists of two parts—Small and Large Sevan—separated by a strait with an underwater threshold between Cape Noraduz (in the west) and Artanish Peninsula (in the east) (Figure 1). A total of 28 small rivers flow into the lake (24 of them into Large Sevan); one river, Hrazdan (a tributary of the Araks River, which is a tributary of the Kura River, flowing into the Caspian Sea) flows from Small Sevan. Small and Large Sevan differ significantly in their morphometric parameters. Until 1933 (the year of the beginning of the artificial reduction of water level in Lake Sevan), the surface areas of Small and Large Sevan were 383.6 and 1032.4 km^2, respectively, and the volumes of water masses were 19.52 and 38.95 km^3, maximum depths were 98.7 and 58.7 m, average depths were 50.9 and 37.7 m, and the drainage basin area was 3475 km^2; the zero level of the lake was on average at an altitude of 1916.2 m in the Baltic elevation system (BS); the maximum length and width of the lake were 75 km and 37 km, respectively [2,3,5,6].

Figure 1. Schematic map of Lake Sevan and distribution of depths in lake (map modified from [1]). Mapped designations: 1—Cape Noraduz, 2—Artanish Peninsula, 3—Cape Tsovinar.

A peculiarity of Lake Sevan is the small ratio (about 2.5:1) between the catchment area (without the lake) and surface area of the lake (for most other large lakes it averages 10:1) [1,5,6], which causes a weak influence of the processes occurring in the drainage basin on the characteristics of the lake itself. Evaporation from the surface of the lake is approximately equal to the main incoming part of its water balance—the sum of the runoff of inflowing rivers and atmospheric precipitation [1,2,5,6]. The idea of reducing the costs of ineffective evaporation and using the released water for national economic purposes (irrigation of the Ararat Valley and generating electricity) formed the basis of the project proposed in 1910 by the Armenian engineer S. Manasserian. This project assumed

a decrease in the lake level by 55 m over 50 years and, accordingly, a reduction in its area to 299 km^2 [1,5,6], which would actually lead to the destruction of Large Sevan using its drained bottom for crops.

In accordance with this project, adopted by the Soviet government, in 1933, an artificial decrease in the level of Lake Sevan began. The bed of the Hrazdan River was deepened and the Sevan–Hrazdan Energy Complex was created [2,3,5,6]. As a result of the intensive use of lake waters for irrigation and energy needs, its level began to decline, especially intensively from 1949 to 1964 (at a rate of up to 1 m/year). Some rise in the level occurred after the commissioning of the Arpa–Sevan tunnel in 1981, through which the water of the Arpa River began to flow into the lake. The minimum level of Lake Sevan (1896.32 m BS, approximately 20 m below natural) was recorded at the end of 2001 [2]. In accordance with "The Law about Lake Sevan" adopted in the Republic of Armenia in 2001, which provided for an increase in the lake level by 2030 to the optimal level of 1903.5 m [7,8], the level began to rise at a rate of 25–45 cm/year [6]. However, a sharp increase in the lake level led to flooding of the shores and buildings of the coastal zone, so in 2011, it was decided to temporarily limit its further growth. In the decade of the 2010s, there were years of relatively small changes in the level of Sevan [8]. By the beginning of 2021, the lake level reached 1900.52 m BS, on 20 July 2022 it was 1900.66 m BS [9], and by the beginning of 2023, it was 1900.27 m [10].

A sharp drop in level and its subsequent increase, accompanied by pollution from flooded shores and the flow of untreated wastewater, led to significant changes in the morphometric, physical, thermal, and biochemical characteristics and ecosystem of the lake [2,5–8,11–14]. Already in 1964, abundant blooms of blue-green algae (cyanobacteria) were observed here, which recurred periodically until the second half of the 1970s and during the decade 2006–2016 [15]. But their particularly intense flowering in the summer–autumn period has been observed from 2018 to the present, which indicates eutrophication of the lake [8,9,16–19].

A sporadic intense phytoplankton bloom (especially of cyanobacteria) in the modern period is observed in many lakes, bays, seas, and oceans (for example, in Lake Villarrica, Chile [20], in the Caspian Sea [21–23], in the Baltic Sea [24], in the Sea of Azov [25], and in the Black Sea [26]). A necessary condition for such flowering is an increase in the concentration of nutrients (phosphorus and nitrogen compounds) in the water. However, local sources of increased concentrations of nutrients are not always known.

For Lake Sevan, the factors that have caused its eutrophication in recent years are associated with artificial changes in its level. This is an increase in the concentration of phosphorus and nitrogen compounds in water (due to river flows, domestic wastewater, agricultural waste, cage fish farming, and numerous resorts, hotels, and restaurants on the shore, and flooding of the untreated coastal zone), an increase in its temperature by about 2 °C as a result of a decrease in the depth of the lake and climate warming, and a decrease in the level of hydrobiological self-purification due to a reduction in the number of inhabitants in the lake (due to overfishing and deterioration of the ecology of the basin). An additional factor contributing to the increase in the concentration of nutrients in the lake water due to a decrease in its level is the reduction in the hypolimnion layer (cold layer below the thermocline) by 50% in Small Sevan and its disappearance in Large Sevan, which leads to the transfer of nitrogen and phosphorus from bottom sediments into the water [2,5,10].

It is obvious that the main sources of nutrients entering the lake waters, leading to intense algae blooms, are concentrated in its littoral zone. This is confirmed by hydrobiological and satellite observations [18,19,27], which showed that large-scale water blooms began in the coastal part of Large Sevan, in particular near the mouths of major rivers, and then extended to deep-water areas. Ocean color satellite images [17,18,28,29] also show that the bloom covers not only the littoral but also the deep-water part of Lake Sevan. The spread of water from the coastal zone of the lake to its deep-water part implies intense horizontal mixing of water in this reservoir. However, the mechanisms of such mixing and

the factors determining them were practically unknown until recently. Studying them is important both from a scientific point of view and from the practical task of monitoring the ecological state of the modern eutrophicated lake.

Even when studying the thermal regime of Lake Sevan in 1926–1930, the existence in the central part of Large Sevan in the summer–autumn period of a dome of cold waters was established, associated with the rise of deep waters into the surface layers [30]. Based on the experimentally established stable existence of this dome for 4.5–5 months even with strong winds, as well as measurements of current speed using several suspended floats in the upper 10 m layer in 1958, M.M. Ainbund concluded that there is a cyclonic circulation of water in Large Sevan [31]. A less intense cyclonic gyre was also discovered in Small Sevan [31]. The cyclonic circulation in Large Sevan was later confirmed by a few data points on surface currents obtained using the method of special postcards [32], as well as later field measurements of current velocities [33] and calculation of currents based on the temperature (density) field using the dynamic method [34].

Organization of instrumental quasi-synchronous measurements of the velocity and direction of currents on the scale of the entire lake with good spatial resolution is practically impossible; therefore, the main methods for studying its circulation are mathematical modeling and analysis of satellite information. In works on the hydrodynamic mathematical modeling of currents in Lake Sevan in the 1970s–1980s [35–38] for the summer season (August) with the wind characteristic of this period, the density field according to temperature observations and the known bottom topography [39] demonstrated, with some differences, a clearly defined cyclonic circulation in Large Sevan on a basin scale and the presence of a cyclonic gyre in Small Sevan, which is consistent with the field observations mentioned above.

However, basin-scale cyclonic circulation does not explain the clearly existing intensive water exchange between the littoral zone and the deep-water part of the lake. As shown by a few field observations and numerical modeling, intra-basin circulation in lakes and small reservoirs, in addition to the typical cyclonic circulation on the basin scale [40] (with the exception of the Aral Sea with anticyclonic circulation [40–42]), includes smaller-scale gyres [33,42]. In this case, the factors determining the circulation of the reservoir are the nature of the wind influence, bottom topography/orography, and water stratification. Analysis of satellite images with a high spatial resolution (optical imagery and SAR images) has made obvious sub-basin eddy dynamics in many bodies of water, including both freshwater (for example, Lake Baikal [43], Lake Superior (North America) [44], Skadar Lake in Montenegro/Albania [45], and Geneva Lake [46]) and hypersaline water (for example, the Kara-Bogaz-Gol Bay of the Caspian Sea [47,48], the western Large Aral Sea [49,50]). Astronaut photographs from the International Space Station [51] showed numerous eddies in saline Lake Van.

The above-mentioned research of water dynamics in different lakes of the world with the use of satellite remote sensing methods has shown that, in general, the methods developed for the ocean surface can be easily applied to the water surface of the lakes, because the physical principles of detection of currents, eddies, dipoles, filaments, and other dynamic structures are the same. They are based on the detection of any color (suspended matter, chlorophyll concentration), thermal (water surface temperature), and/or surface roughness contrasts at the water surface. Of course, different lakes are located at different altitudes, and in contrast to the ocean, mountain lakes may need a different atmospheric correction procedure. Lakes can be very shallow, and, in these cases, the bottom may have a significant impact on the signal received by a satellite from the water surface. Lakes can have significant values of suspended matter concentration and floating vegetation that may impact water-leaving radiance and brightness temperature. In these cases, standard algorithms for ocean color data processing and water temperature retrieval should be modified to take into account local peculiarities.

We recently demonstrated intense eddy dynamics in Lake Sevan using optical satellite images [28,29]. This research has shown that there are several challenges in processing

satellite images of Lake Sevan in the optical and infrared spectral bands because of a lack of optical (suspended matter and chlorophyll concentration) and thermal (surface water temperature) contrasts for most of the year. Therefore, to investigate mesoscale and submesoscale water dynamics in the lake, it is necessary to process each optical image individually with the help of different combinations of spectral bands to display better vortices at the lake's surface. Second, it became clear that the use of Synthetic Aperture Radar (SAR) satellite images with a spatial resolution of about 10 m can help significantly because (1) SAR is based on other physical principles and does not need optical and temperature contrasts on the water surface, and (2) the advantage of satellite radar compared to the optical and thermal sensors is all-weather survey regardless of cloud cover and sun illumination (day/night).

The main goal of this work is to study the variability of the horizontal circulation of the surface layer of Lake Sevan based on the analysis of a larger array of optical and radar satellite images with high spatiotemporal resolution in different months and different years (2017–2022). In addition, in view of the importance of current information about the level of the lake (and, accordingly, its surface area and water volume), which only occasionally appears in publications, the possibility is considered of using time sequences of the morphometric parameters of Lake Sevan, available in the near-real time HYDROWEB database, developed and maintained at the Laboratory of Space Geophysical and Oceanographic Studies (LEGOS), France [52,53], to monitor the progress of changes in these parameters in the modern period for hundreds of lakes in the world.

2. Data and Methods

2.1. Satellite Optical and SAR Images

To study the horizontal circulation of water in the surface layer of Lake Sevan, we analyzed high-resolution satellite ocean color data (10 m) MSI Sentinel-2A, -2B True Color images (https://apps.sentinel-hub.com/eo-browser, accessed on 19 January 2024) in the summer–autumn period for 6 years (2017–2022), with a frequency of mainly 5 days. To illustrate the variability of water circulation in Lake Sevan, we selected images from different years from July to October—during the period of thermal stratification of waters and intense phytoplankton bloom. In cases where sequential informative images (with an interval of 5–10 days) are available in the data set, they are presented to illustrate the time scale of variability of the eddy pattern.

The passive tracer of surface currents in these images is phytoplankton, the presence of which on the surface or in the near-surface layer changes the color of the water and, accordingly, affects the scattered signal [54–56]. Note that the biomass of different types of phytoplankton (cyanobacteria, green algae, and diatoms) in different months of the warm season in Lake Sevan is different [17], and in most cases we do not know what type of phytoplankton was a tracer on satellite images in each specific case, with the exception of July 2018, when, according to [16–18], cyanobacteria dominated in the algal community.

As an additional means of obtaining information about the elements of the horizontal circulation of the lake, informative radar images, which are closest in date to the analyzed True Color Data, were also used. Synthetic Aperture Radar (SAR) images from the Sentinel-1A, -1B satellites (spatial resolution—10 m, periodicity—from 1 to 6 days) were obtained from the website https://scihub.copernicus.eu/dhus, accessed on 19 January 2024. The advantage of satellite radar compared to the optical range of the spectrum is an all-weather survey (independent of cloud cover and time of day). The manifestation of eddy structures on the water surface occurs due to the involvement in the eddy movement of slick stripes formed by films of surfactants as a result of phytoplankton blooms (in this case) and dampening the gravity–capillary component of surface waves. Examples of detection of both mesoscale and submesoscale eddies in seas and lakes on radar images can be found in numerous publications (for example, [44,46,54,57–64]). The best range for the manifestation of eddy structures in radar images is the wind speed range of 2–8 m/s over the studied water area [57,60,63].

Radar images also provide information about the local direction and relative intensity of wind forcing on the water surface: areas with a calm (undisturbed) water surface correspond to low values of the backscattered radar signal and, accordingly, dark areas on the radar image; areas with a rough surface correspond to higher values of backscattered signal and bright areas on the radar image [54].

Since Lake Sevan is located at an altitude of 1900 m and is surrounded on all sides by mountains, it is not possible to use satellite data (optical images) with the standard method of processing recommended for ocean color to determine the parameters of geophysical processes, in particular, the detection of eddies on the lake surface. Vortex structures in Lake Sevan appear on both radar images and ocean color images only during intense algae blooms, primarily cyanobacteria. In radar images, they appear due to biogenic films that are captured by surface currents, and in ocean color data due to changes in the spectral brightness coefficients of water-leaving radiance. Therefore, to visualize vortex processes, it is necessary to process each image individually and use a different technique for each image. For MSI Sentinel-2 data we used both the second-level data, for which atmospheric correction is carried out according to the standard method, and the Dark Spectrum Fitting algorithm that we applied to the first-level data, which is part of the ACOLITE software package (ACOLITE 20231023.0) [65].

Analysis of the results obtained using various atmospheric correction algorithms showed that the choice of algorithms does not affect the visualization of vortex processes. The most important factor when identifying eddies based on satellite data is the depth at which the algae accumulations are located. If they are not located directly on the surface and do not create a biogenic film, there will be no manifestations of vortices on radar images. When using ocean color data, the depth of the algae is also important. Since Lake Sevan is a fairly large body of water, in different areas, algae can be located at different depths. To obtain a more complete picture, it is necessary to use various methods. So, for example, for the MSI Sentinel-2B image from 11 July 2018 (see Section 3.1.2), in which the southeastern part of Large Sevan is very different from the rest, when highlighting this area by changing the range of the spectral brightness coefficient, the rest of the image becomes less suitable for the detection of vortex structures. At the same time, if we additionally use a combination of the NIR-RED-0.22*(SWIR-RED) channels, which gives the Floating Algae Index, the areas where algae are on the surface are reflected most clearly.

For each MSI Sentinel-2 image, it was necessary to select a different range of reflectance (spectral brightness) to have a better view of vortices at the lake surface. For example, for the image from 23 October 2020, which with a standard range of reflectance from 0 to 0.2 does not show any information about vortex processes, the ranges red 0.02–0.05, green 0.035–0.075, and blue 0.08–0.11 were selected, due to which the vortex pattern became clearly visible (see Section 3.1.4).

2.2. Morphometric Parameters of the Lake

Figure 1 gives an idea of the spatial scale of Lake Sevan and its bathymetric/orographic features. The length of the entire lake along the axis from northwest to southeast is about 73 km (the length of Large Sevan along this axis is about 40 km), the maximum horizontal width of Large Sevan is about 36 km, the distance between the southern tip of the Artanish Peninsula and the southern shore of Large Sevan is 33 km, and the width of the strait between Small and Large Sevan is 5.5 km. Large Sevan, in contrast to Small Sevan, has a mostly flat bottom and slight ruggedness of the coastline (with the exception of Cape Tsovinar and the Artanish Bay). Note that the schematic map in Figure 1 is apparently a simplified version of a detailed bathymetric map based on the results of a hydrographic survey of 1928–1930, i.e., before the start of the artificial drainage of the lake waters [39] (due to the complexity of this detailed map, it is not possible to present it in this article). Accordingly, the depths shown in Figure 1 do not correspond to the modern level of the lake (approximately 1900.5 m BS, i.e., approximately 16 m below natural). Thus, if on the bathymetric map corresponding to the natural state of the lake [39], the depths of the

central part of Large Sevan within the 40 m isobath varied mainly from 40 to 50 m (with the exception of several point depressions with a maximum depth of 58.7 m), then in the modern deep-water part of this basin, the depth range would be approximately 24–34 m. In the southeastern part of Large Sevan, the depths smoothly decrease from approximately 24 m to the shore.

Information about the morphometric parameters of Lake Sevan since 1995, based on data from satellite altimetry, optical satellite imagery, and algorithms for processing this satellite information developed in the LEGOS laboratory (France) [52,53], can be obtained in the near-real time HYDROWEB database (https://hydroweb.theia-land.fr/hydroweb/view/L_sevan?lang=fr, accessed on 25 January 2024) approximately a week after receiving satellite data [52]. This database contains time series of monthly averages (graphical representation) and digitized intramonthly values of level from 18 June 1995, surface area from 18 June 1995, and volume increments from 7 July 1995 (relative to some reference value for 18 June 1995) to 15 January 2024. The calculated values of the surface area and volume increments from January 1999 to April 2002 are presented in the database with large gaps; in subsequent years, there are no such gaps. The number of annually measured/calculated values of level, surface area, and volume increments relative to some reference value in the HYDROWEB database varies from 6 to 14 in the period from 1995 to 2019, and since 2020, it has increased to 44–52.
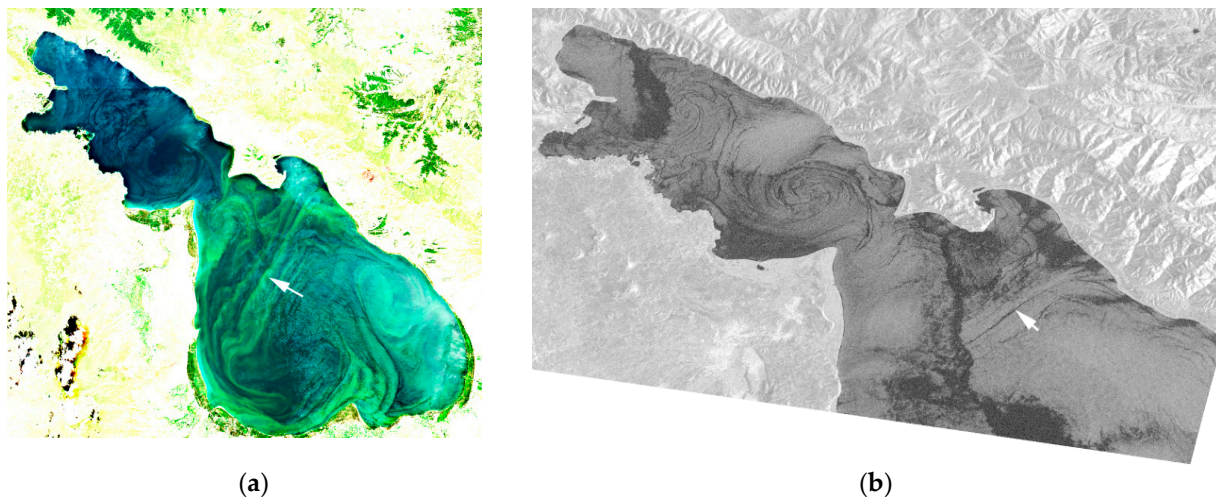
To understand the possibility of using the HYDROWEB database not only for a qualitative analysis of the nature of changes in the morphometric parameters of a lake over time but also for their quantitative assessment, it is necessary to compare the data from this database with the corresponding results of instrumental measurements. Regular measurements of the level of Lake Sevan are carried out at gauging stations, and the corresponding values of the surface area and water volume are determined from the known distributions of these parameters over depth, based on detailed bathymetry of the bottom [39], or from hypsometric curves constructed in accordance with these distributions (for example, Figure 1.3.1.1 in [12]). These in situ data, published in [2,6,9,12] and others published from time to time in different sources accessible via the Internet, were used to validate the values of morphometric parameters in the HYDROWEB database.

3. Results

3.1. Manifestation of Eddy Dynamics on Satellite Images

3.1.1. August 2017

In Figure 2a, in the center of the deep-water part of Large Sevan, we can distinguish a cyclonic (anticlockwise) gyre ($\approx$18 km) with attached anticyclonic (clockwise) eddies in the western ($\approx$5 km), eastern ($\approx$9 km), and southern ($\approx$4 km, behind Cape Tsovinar) sections of the periphery. The attached anticyclone in the western part of the basin branches into a smaller dipole (a combination of two eddies of opposite rotation with a jet between them; eddy size $\approx$ 3 km, an area south of the strait). In Small Sevan, a cyclonic gyre appears near the strait ($\approx$9 km) with attached elements of anticyclonic vorticity on its southeastern and northwestern sides ($\approx$3 km) and a cyclonic eddy ($\approx$4 km) north of this tripole. This cyclonic gyre with an attached anticyclone, partially located in the strait, and a straight part of the western periphery of the cyclonic gyre in Large Sevan (marked by an arrow) are clearly visible on the radar image the day before (Figure 2b). There is a noticeable turn of this straight part of the cyclone periphery in the cyclonic direction between 19 and 20 August 2017.
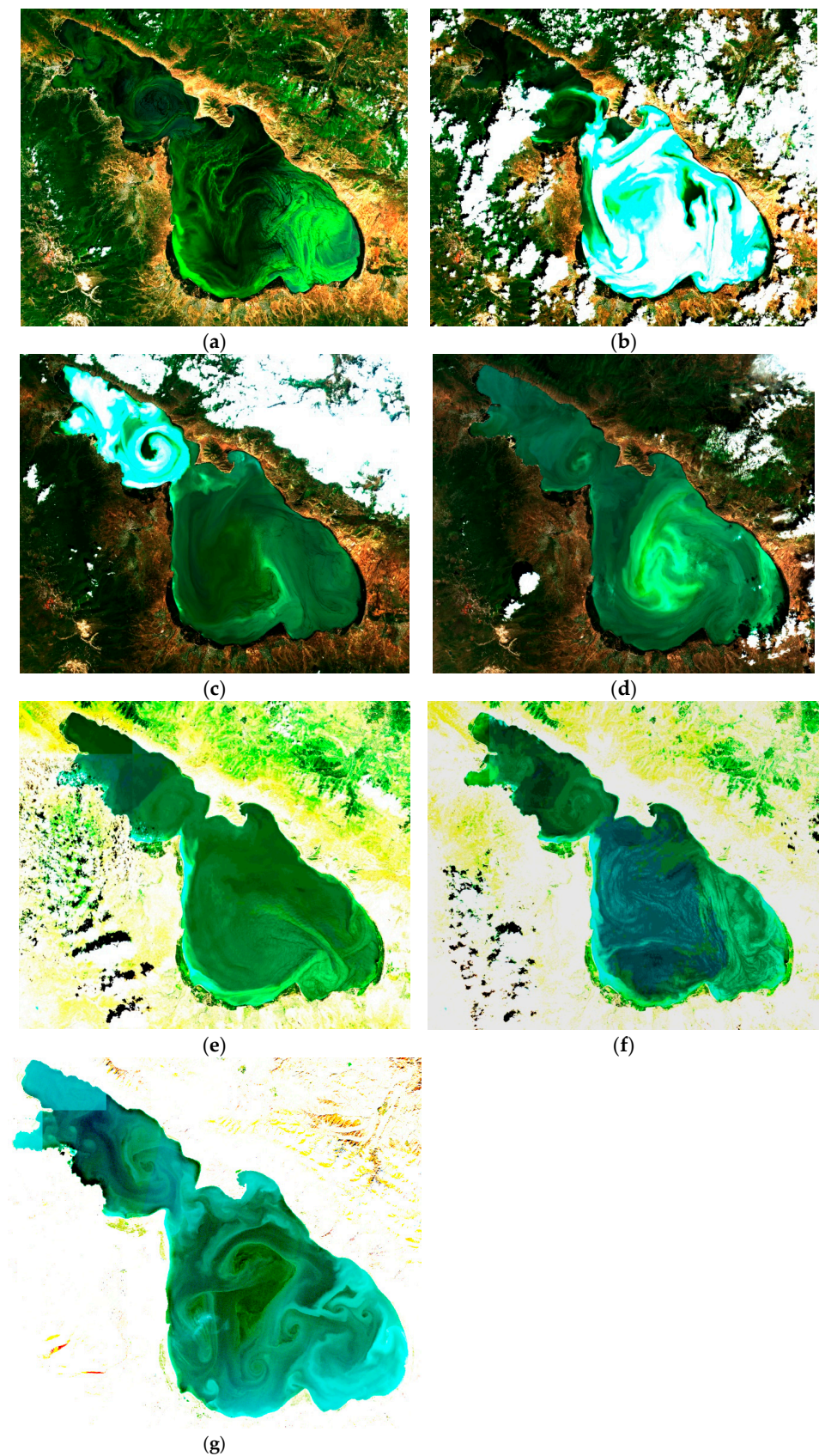
(**a**)   (**b**)

Figure 2. Eddy dynamics in Lake Sevan in August 2017: an MSI Sentinel-2A image on 20 August (**a**) and a SAR-C Sentinel-1B image on 19 August (**b**). The arrows show the positions of the straight section of the western periphery of the cyclonic gyre in Large Sevan. Lighter tones in Figure 2a corresponds to a higher concentration of phytoplankton (chlorophyll), in Figure 2b—to higher wind speed.

3.1.2. July–October 2018

July 2018 was the period of the most intense phytoplankton bloom (mainly cyanobacteria [17,18]) for the entire period under consideration, with the highest water surface temperatures in July for the period 2009–2018 [17]). On 11 July (Figure 3a), flowering was most intense in the shallow southeastern part of Large Sevan, on 21 July (Figure 3b), it covered the entire Large Sevan, after 5 days it was observed in Small Sevan (Figure 3c), and after another 5 days, a cluster of flowering algae was visible in the cyclonic gyre of Large Sevan and in its southeastern littoral zone (Figure 3d).

On 11 July (Figure 3a), the cyclonic gyre in the deep-water part of Large Sevan had not yet manifested itself. Elements of horizontal circulation in Small Sevan were clearly visible: a cyclonic gyre north of the strait (≈9.5 km) and a combination of mushroom-shaped currents in the northern part of the basin. After 10 days, on 21 July (Figure 3b), during the most intense water bloom in Large Sevan, the cyclonic eddy (≈24 km in the meridional direction and 16 km in the latitudinal direction) with elements of anticyclonic vorticity in its southern, western, northern and eastern parts of the periphery occupied almost the entire deep-water part of this basin. In the shallow southeastern part of Large Sevan, one can assume the presence of an eddy dipole, which was clearly visible in the optical image five days later (Figure 3c). The presence of a cyclonic gyre in Small Sevan on 21 July (Figure 3b) can be judged by the waters with an increased content of phytoplankton from Large Sevan involved in its vortical movement, while five days later (Figure 3c), this gyre with an attached anticyclonic eddy on its northwestern part of the periphery was clearly visible in the field with an increased phytoplankton bloom. In Large Sevan, at the same time (Figure 3c), there was a cyclonic gyre in the deep-water basin, an anticyclonic eddy behind Cape Tsovinar, and an eddy dipole with a jet part oriented to the west (the size of the eddies was ≈9 km) in the shallow southeastern part. The distribution of waters with an increased concentration of phytoplankton in the northern part of Large Sevan from its western shore to the Artanish Bay indicates local circulation in an anticyclonic direction. Over the next five days (31 July), the main elements of deep-water circulation were maintained (Figure 3d).

Figure 3. Manifestation of variability of eddy dynamics in Lake Sevan in July–October 2018 on MSI Sentinel-2 images: 11 July (**a**), 21 July (**b**), 26 July (**c**), 31 July (**d**), 25 August (**e**), 30 August (**f**), and 29 October (**g**).

By 25 August 2018 (Figure 3e), the pattern of vortical movements had changed noticeably. The cyclonic gyre (dimensions in the latitudinal and meridional directions ≈ 23 and 13 km, respectively) in Large Sevan occupied only the southern part of the deep-water basin, forming a packing with a slightly smaller anticyclone to the north of it and a mushroom-shaped structure behind Cape Tsovinar. A cyclonic eddy was seen in the eastern shallow part of Large Sevan, and a cyclonic gyre appeared in Small Sevan. Five days later (Figure 3f), a packing of two eddy dipoles was observed in Large Sevan with a common cyclonic eddy in the center (≈12 km) and anticyclones to the north and south of it (the size of the eddy structure in the latitudinal direction was ≈20 km). The size of the cyclonic gyre had thus decreased significantly. In the southeastern part of Large Sevan, there was a complex picture of multi-scale cyclonic and anticyclonic vortices with a maximum size of ≈6 km. In the Artanish Bay, there was a cyclonic eddy (≈4 km). A cyclonic gyre remained in Small Sevan. It also appeared (with a reduced diameter and attached anticyclonic eddies) at the end of October, when, in Large Sevan, only numerous eddies were visible, mainly cyclonic, with the largest in the center of the deep-water basin, and an eddy dipole in the southeastern part (Figure 3g).

3.1.3. July–October 2019

On the satellite image of 11 July 2019 (Figure 4a), in Large Sevan, the following were clearly seen: an eddy dipole with an approximately horizontal jet part of the westerly direction between the cyclone (to the south) and the anticyclone (to the north), occupying the entire deep-water part of the basin; an eddy dipole near the Artanish Peninsula, which is a branch of the anticyclonic part of the deep-water eddy dipole; a small anticyclonic eddy behind Cape Tsovinar; an eddy dipole in the shallow southeastern part of the lake. The cyclonic part of the eddy dipole in the deep-water part of Large Sevan (size in the latitudinal direction is approximately 21 km, in the meridional direction—13 km) formed an eddy packing with an anticyclone behind Cape Tsovinar (≈5 km) and a dipole in the southeastern part of the lake (vortices measuring ≈ 5 km). The existence of cyclonic circulation in Small Sevan is confirmed by the stream of phytoplankton-rich waters from Large Sevan involved in the cyclonic movement.

Five days later, on 16 July (Figure 4b), most of Large Sevan was occupied by a dipole structure of a deep-water cyclonic eddy (≈21 km) and an anticyclone in the shallow southeastern region (horizontal size was ≈10 km). In this case, the deep-water cyclone included two smaller cyclonic eddies (≈7 km) connected by a jet, clearly interacting. The dipole was also observed in the Artanish Bay (eddies ≈ 3 km). The same interconnected cyclonic eddies in the deep-water cyclonic gyre of Large Sevan, as ten days earlier, but with changing orientation, were observed in Large Sevan on 26 July (Figure 4 in [29]). On 31 July (Figure 4c), in the cyclonic gyre, a chaotic tracer distribution can be seen instead. At the same time, at the northern periphery of the cyclone, there was an element of anticyclonic vorticity, ending with a cyclonic eddy in the Artanish Bay, and at the southern periphery of the deep-water cyclone, there was an anticyclone extended along the coast. In the southeastern part of Large Sevan, there was an eddy dipole, the anticyclonic component of which (≈10 km) also formed a dipole with a deep-water cyclone. The cyclonic gyre, which occupied almost the entire deep-water part of Large Sevan, was observed on optical (5 August, Figure 4d), 10 August (Figure 7a in [29]), 15 August (Figure 4e), and radar (Figure 4f) images.

Very variable eddy dynamics of waters in Large Sevan were observed in September 2019. The dynamic situation in its deep-water part on 14 September (Figure 4g) is similar to what took place on 25 August 2018 (Figure 3e) and 11 July 2019 (Figure 4a): a horizontally oriented dipole (two-cell circulation) with a cyclonic gyre in the southern part and an anticyclonic eddy of approximately the same scale to the north of it. A small cyclonic eddy (≈3 km) near the Artanish Peninsula, involving water from Small Sevan and ensuring its transfer to Large Sevan, is an attached eddy on the periphery of this large anticyclonic formation. In the southeastern part of the lake, a cyclonic eddy or dipole appeared with a jet part directed to the northwest.
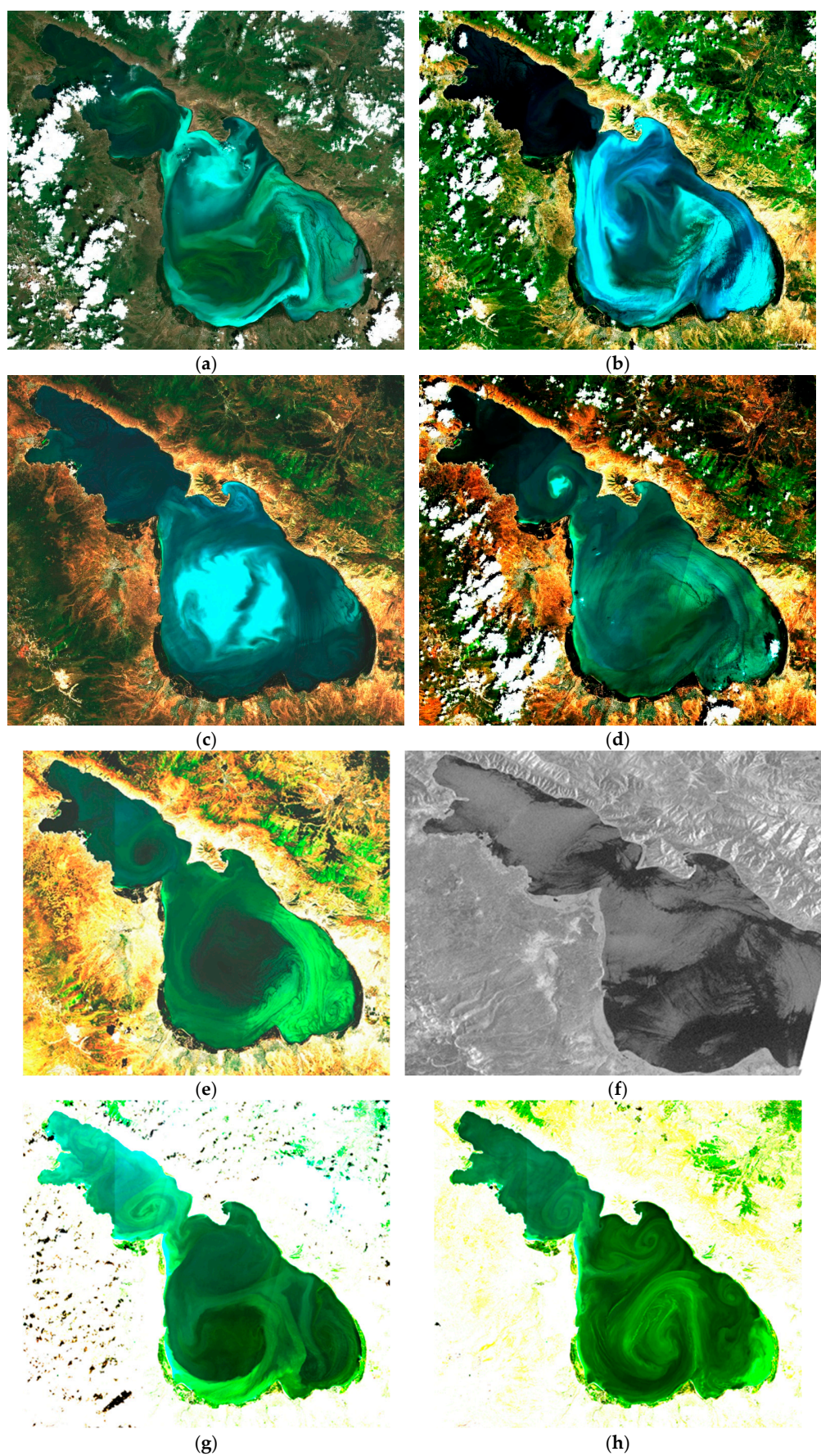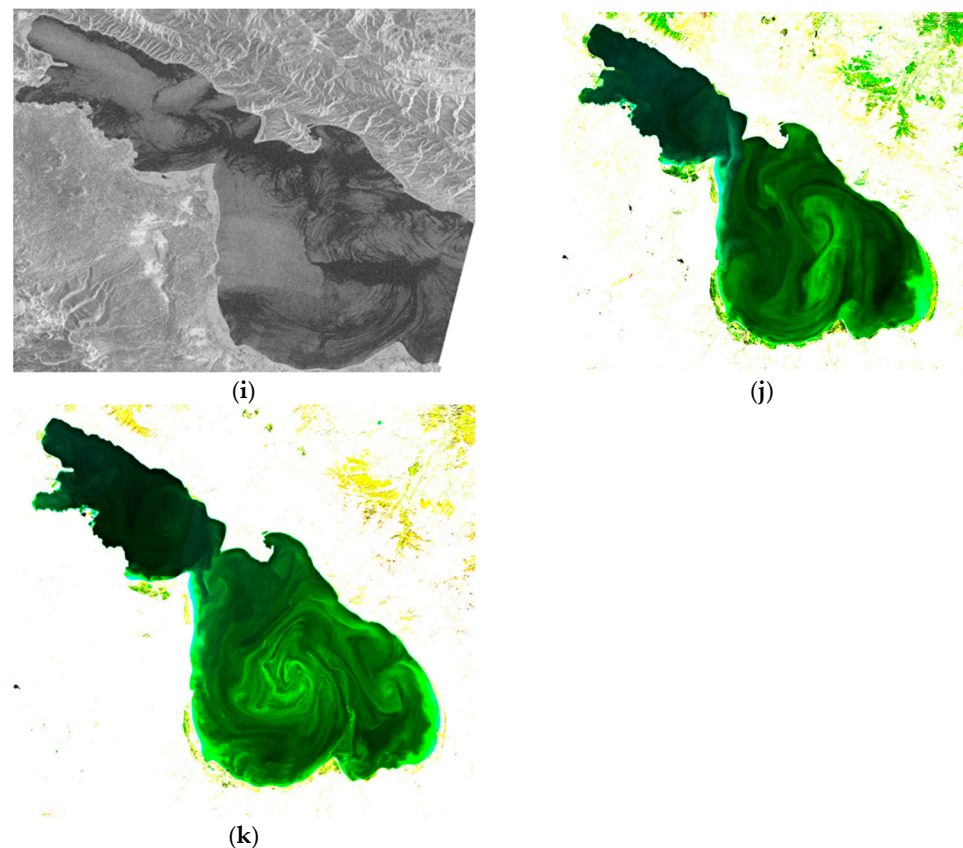
(a)

(b)

(c)

(d)

(e)

(f)

(g)

(h)

Figure 4. *Cont.*

(i)

(j)

(k)

Figure 4. Manifestation of variability of eddy dynamics in Lake Sevan in July–October 2019 on MSI Sentinel-2 images: 11 July (**a**), 16 July (**b**), 31 July (**c**), 5 August (**d**), 15 August (**e**), 14 September (**g**), 19 September (**h**), 24 September (**j**), and 14 October (**k**); and SAR-C Sentinel-1A images on 15 August (**f**) and 20 September (**i**).
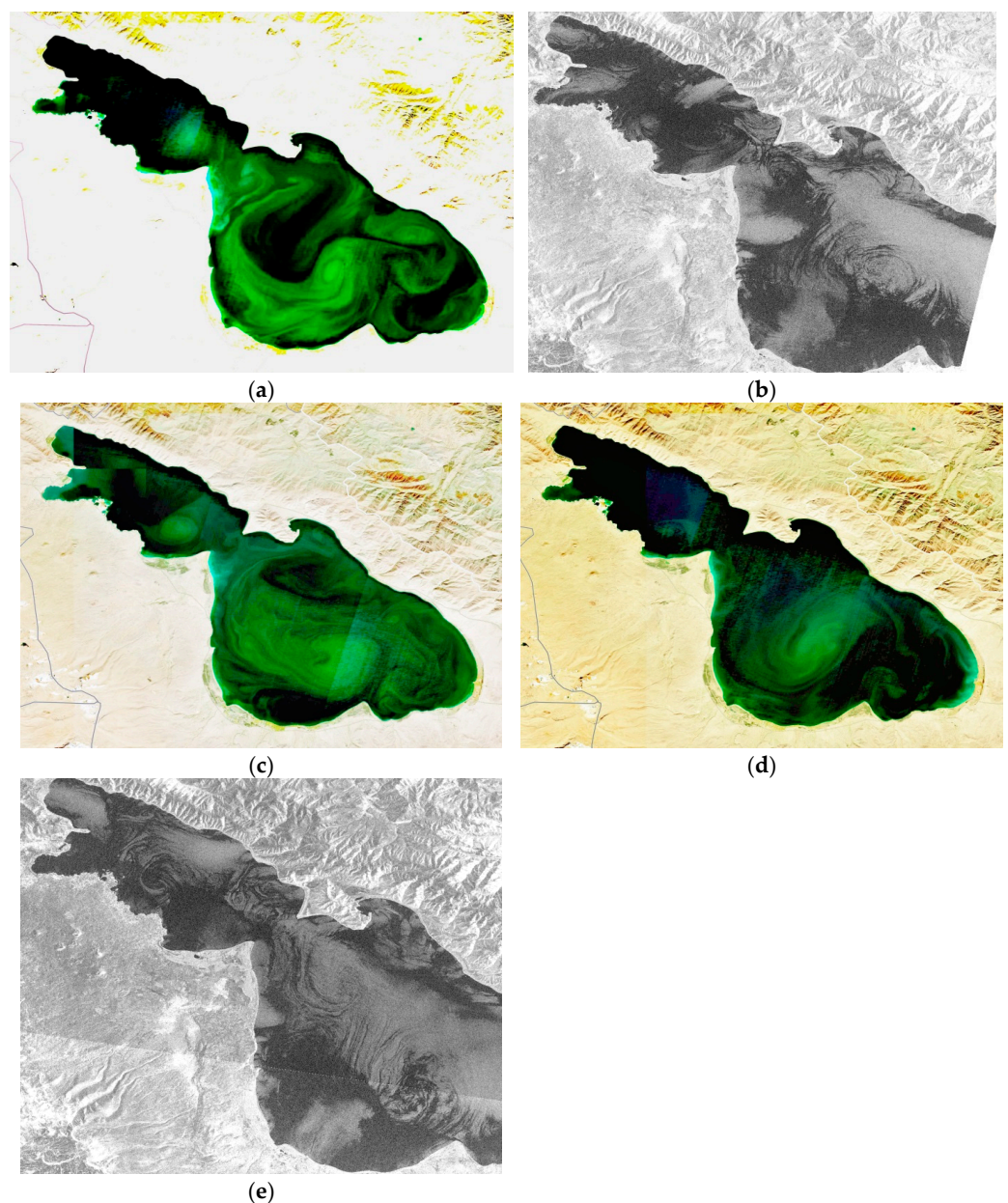
Five days later, on 19 September (Figure 4h), the picture changed dramatically. The southern deep-water part of Large Sevan was occupied by a cyclonic gyre (maximum size ≈ 20 km) with a small element of anticyclonic vorticity on the western part of the periphery. This cyclone eddy formed a packing with an eddy dipole in the eastern part of the basin (eddy sizes of ≈ 5 km). Between this dipole, oriented to the east, and the coast, one can see a small dipole (eddy sizes ≈ 2.5 km) with an axis in the western direction (perhaps, this was the mushroom-shaped flow of the Masrik River). In the northern part of Large Sevan, a packing of mushroom-shaped structures with mutually perpendicular axes was visible. The cyclonic part of one of these structures (≈6 km), located near the Artanish Bay, was connected by a jet with a cyclonic gyre located to the south. Some of the eddy structures observed a day later appeared in the radar image (Figure 4i).

By 24 September (Figure 4j), the water circulation had changed again. Now, the central figure of the deep-water part of Large Sevan was a dipole with a vertical axis in a southern direction, and the cyclonic part of the dipole represented two interconnected cyclonic eddies of a smaller size (≈7 km). The northern of these cyclones formed a packing with an anticyclonic eddy (or part of a dipole) in the eastern part of the basin. It appears that by 14 October (Figure 4k), the structure of the cyclonic gyre (with merged smaller cyclones) and the dipole in the eastern part of the basin had turned in the cyclonic direction, and the deep-water basin was now occupied by the dipole of this cyclonic gyre and the anticyclonic eddy to the west of it with the jet part of the south–west direction between them. A small cyclonic eddy in the northern part of Large Sevan near the strait was involved in the movement of water both from the western shore of Large Sevan and from Small Sevan near the eastern shore of the strait. In the Artanish Bay, there was a cyclonic eddy (≈4 km).

3.1.4. October 2020

On 13 October (Figure 5a), a cyclonic eddy with a size of approximately 9.5 km northwest of Cape Tsovinar was clearly visible in Large Sevan, forming a packing with an eddy dipole in the eastern part of the basin (the size of the eddies was about 7 km). Small dipoles were also visible in the shallow southeastern part of the basin (eddies ≈ 3 km in size) and south of the strait (eddies ≈ 3 km in size). We can assume the presence of an anticyclone to the west of this cyclonic eddy (judging by the presence of shear cyclonic instability elements on the northern periphery of the flow directed northeast to the Artanish Bay) and a small cyclonic eddy in the bay itself. The area with increased phytoplankton content in Small Sevan corresponded to the cyclonic gyre, which, together with the associated anticyclonic eddy on its eastern periphery, appeared on the radar image a day later (14 October, Figure 5b). The same radar image clearly showed the increased size of the cyclonic gyre north of Cape Tsovinar in Large Sevan.

Figure 5. Eddy dynamics in Lake Sevan in October 2020 on MSI Sentinel-2 images on 13 October (**a**), 18 October (**c**), and 23 October (**d**), and SAR-C Sentinel-1 images on 14 October (**b**) and 26 October (**e**).

Four days later (18 October, Figure 5c), most of Large Sevan was occupied by a zonally oriented eddy dipole from this cyclone (≈20 km in the latitudinal direction and 11 km in the meridional direction) and the anticyclone to the north of it (≈17 and 9 km, respectively). It was also possible that another anticyclonic eddy was located between the cyclonic part of the dipole and the southern coast of the basin west of Cape Tsovinar. In this way, a three-cell structure was formed in the deep-water part of Large Sevan. The entire southeastern part of Large Sevan east of Cape Tsovinar was occupied by a smaller-scale eddy dipole. A cyclonic eddy (≈4 km) in the Artanish Bay was seen as well as a small cyclone (≈3 km) in the strait near the Artanish Peninsula, along the periphery of which water from the western coast of the northern part of Large Sevan spread to Small Sevan.
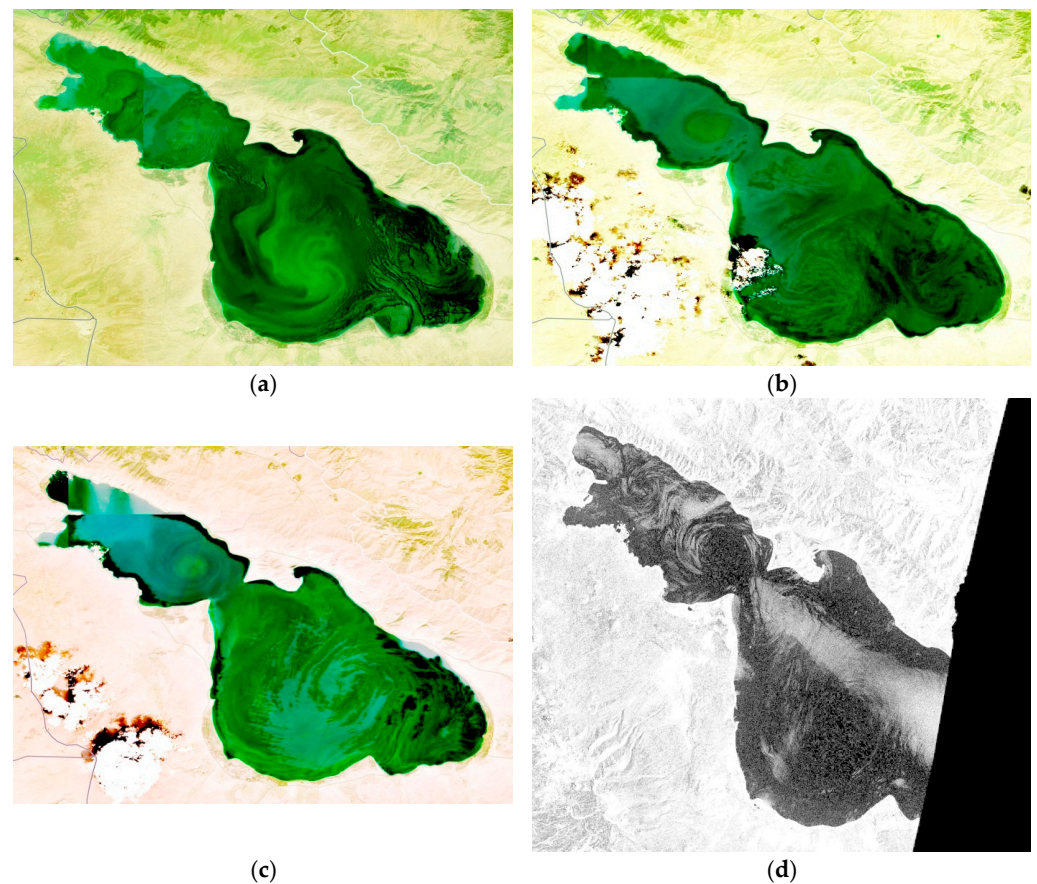
After another five days (23 October, Figure 5d), the eddy dipole in the central part of Large Sevan appeared to have rotated approximately 45 degrees counterclockwise. The outlines of the dipole structure in the southeastern part of the basin, associated with the cyclonic gyre, were preserved, and a small dipole was visible at Cape Tsovinar. In Small Sevan, there was a cyclonic eddy (about 5 km). The radar image three days later (26 October, Figure 5e) showed a cyclonic gyre west of Cape Tsovinar and a smaller cyclonic eddy in the northern part of Large Sevan. Judging by the outlines of the stripes south of the latter, one can assume the presence of an anticyclonic eddy in the shaded area of the radar image. In this case, there would be a packing of two dipoles (mushroom-shaped currents) with southern and eastern directions of jets between eddies of opposite directions of rotation. In Small Sevan, near the strait, there was a group of small-scale cyclones. To the north of this group, a mushroom-shaped structure can be seen, the eastern part of the periphery which coincided with the southern border of the eastern wind flow.

3.1.5. August–September 2022

The optical image on 14 August (Figure 6a) showed a difficult-to-interpret eddy structure with a clearly expressed element of cyclonic vorticity (possibly a dipole) in the deep-water Large Sevan, an anticyclone behind Cape Tsovinar, and a dipole in the southeastern part of the basin with a southerly direction jet between the eddies of the pair. In Small Sevan, there is a cyclonic eddy (≈6.5 km) and two eddy structures (≈3 and 4.5 km) in the northern part, the direction of rotation of which cannot be determined.

Two weeks later (29 August, Figure 6b), the southern part of Large Sevan was occupied by a dipole of a cyclonic eddy (≈9 km), located approximately in the same place as in Figure 6a, and an anticyclone between it and the coast. This cyclonic eddy was connected by a jet to a cyclone (≈6 km) in the Artanish Bay. In the eastern part of the basin, there was a packing of two mushroom-shaped currents with mutually perpendicular jets in the southwestern and southeastern directions (the size of the eddies was ≈4–5 km). The entire southern part of Large Sevan was a system of interconnected eddies.

After another five days (3 September, Figure 6c), most of the deep-water basin appeared to be moving in a large dipole structure, with a cyclone and an anticyclone each approximately 20 km in size and a jet between them oriented to the southwest. In this case, the anticyclonic part of the dipole branched into a smaller dipole (the vortices of the pair were ≈ 3 km). To the east of the cyclone, there appeared to be another anticyclone, and thus the movement of waters throughout Large Sevan was determined by this tripole structure. These eddy structures, as well as the cyclonic gyre (8 km) and the package of mushroom-shaped currents to the northwest of it in Small Sevan, were clearly visible in the radar image (Figure 6d).
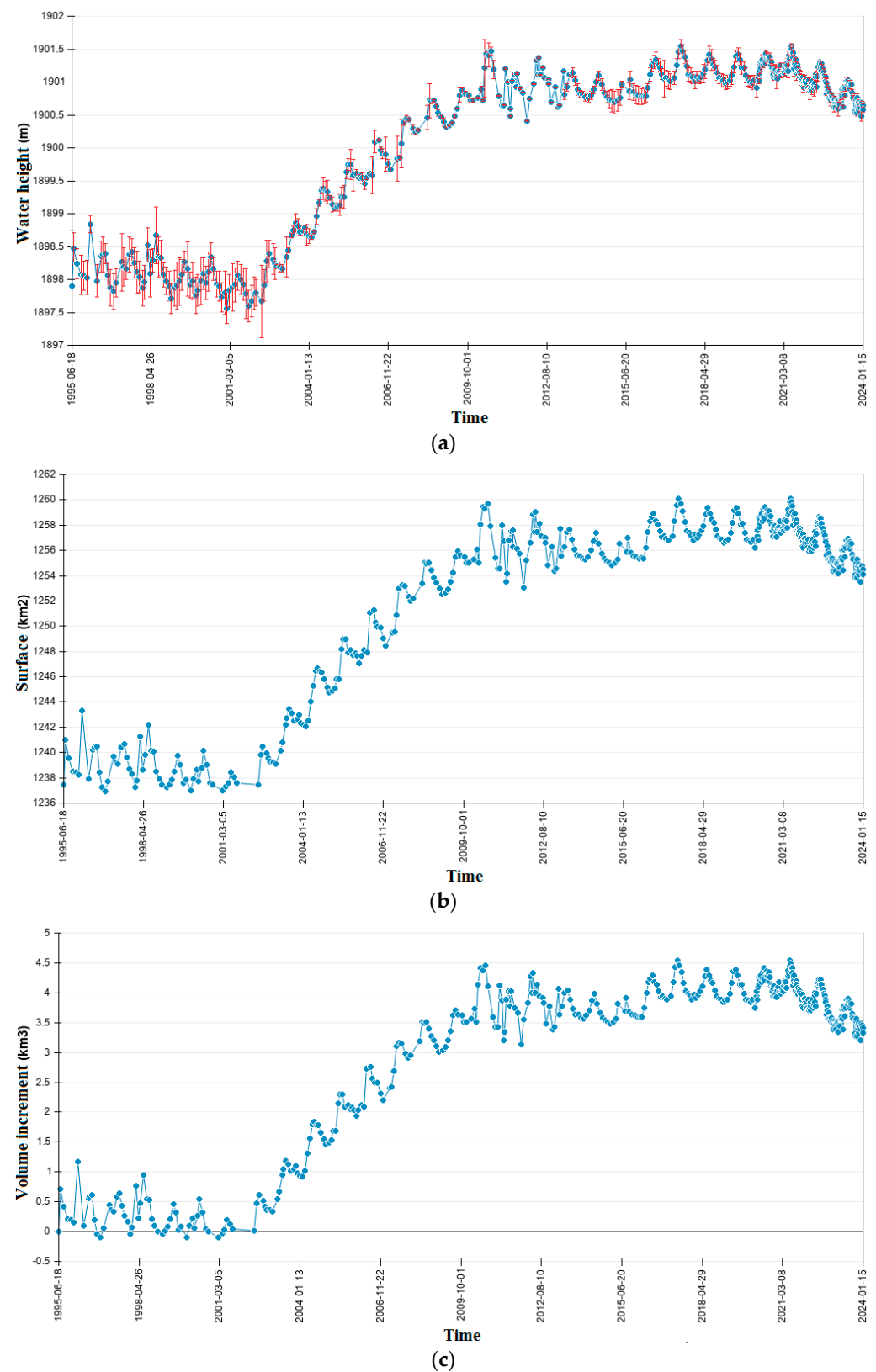
Figure 6. Eddy dynamics in Lake Sevan in August–early September 2022 on MSI Sentinel-2 images on 14 August (**a**), 29 August (**b**), and 3 September (**c**), and SAR Sentinel-1 images on 4 September (**d**).

3.2. Morphometric Parameters of Lake Sevan According to HYDROWEB Data and Measurements at Gauging Stations

The changes in the average monthly values of morphometric parameters of Lake Sevan according to HYDROWEB data for approximately 27.5 years (18 June 1995–15 January 2024) are shown in Figure 7. It can be seen (Figure 7a) that from 1995 to 2001, the lake level decreased (minimum—1897.56 m BS on 15 January 2001), then grew at an average rate of approximately 40 cm/year until 2010 (maximum—1901.47 m BS on 15 August 2010); further, there were years with a slight decrease in the level (2011–2015) and relative stabilization (2016–2021). Since 2021, there has been a decrease in the lake level by about 20 cm/year: on 27 January 2021, the level was 1901.13 m BS, on 23 January 2022—1900.91 m BS, on 29 January 2023—1900.7 m BS, and on 15 January 2024—1900.58 m. Thus, according to altimetry data, by the beginning of 2024, the level of Lake Sevan was 15.6 m below natural (1916.2 m BS). The same nature of change is observed in the surface area and water volume (Figure 7b and Figure 7c, respectively).

The pattern of lake level changes from 1995 to 2020–2021 (Figure 7a) is qualitatively in good agreement with changes in average annual level values during the same period [8,66]. The results of the quantitative correspondence of level values in different years according to HYDROWEB and gauging stations are presented in Tables 1–3.

Figure 7. Time sequences of average monthly values of level from 18 June 1995 (**a**), surface area from 18 June 1995 (**b**), and volume increments from 7 July 1995 (**c**) to 15 January 2024 of Lake Sevan according to HYDROWEB, LEGOS (France). Red segments in (**a**) are standard deviations.

Table 1. The level of Lake Sevan on January 1 of each year according to the work ([2], Table 4) (in situ), the altimeter on the date closest to the beginning of the year (indicated in brackets) (altimeter), and the difference between them (Δalt–in situ), m.

Year	Water Level, m		Δalt–In Situ, m
	In Situ	Altimeter	
1995	1896.81	1897.90 (18.06)	1.09
1996	1896.75	1898.84 (16.02)	2.09
1997	1896.69	1897.95 (15.01)	1.26
1998	1896.74	1897.87 (01.01)	1.13
1999	1896.62	1897.71 (12.01)	1.09
2000	1896.51	1897.83 (06.01)	1.32
2001	1896.46	1897.56 (15.01)	1.10
2002	1896.32	1897.79 (10.01)	1.47
2003	1896.76	1898.17 (19.01)	1.41
2004	1897.24	1898.66 (15.01)	1.42
2005	1897.65	1899.10 (19.01)	1.45
2006	1898.07	1899.45 (11.01)	1.45
2007	1898.25	1899.84 (18.03)	1.59
2008	1898.79	1900.46 (16.04)	1.67
2009	1898.86	1900.34 (10.02)	1.48
2010	1899.23	1900.76 (17.02)	1.53
2011	1899.905 *	1900.65 (19.01)	0.745

* Adjusted assessment by the State Committee of the Republic of Armenia on Geodesy and Cartography (see [2]).

Table 2. The level of Lake Sevan (as of January 1 of each year, with the exception of specific dates) according to the work [9] (in situ), the altimeter for the closest date (indicated in brackets) (altimeter), and the difference between them (Δalt–in situ), m.

Year/Date	Water Level, m		Δalt–In Situ, m
	In Situ	Altimeter	
2012	1900.13	1900.97 (18.02)	0.84
2013	1900.10	1900.62 (03.01)	0.52
2014	1900.16	1900.77 (07.01)	0.61
2015	1900.13	1900.69 (25.01)	0.56
2016	1900.19	1900.78 (13.01)	0.59
2017	1900.46	1901.03 (01.01)	0.57
2018	1900.42	1901.08 (14.01)	0.66
2019	1900.39	1900.98 (28.01)	0.59
2020	1900.43	1900.99 (14.01)	0.56
2021	1900.52	1901.14 (03.01)	0.62
20 July 2021	1900.75	1901.2 (18.07)	0.45
2022	1900.43	1900.97 (13.01)	0.54
20 July 2022	1900.66	1901.18 (21.07)	0.52

Table 3. The level, area, and volume of Lake Sevan (at the beginning of each year) according to works ([12], Table 1.3.3.1; [6], Table 6.2) (in situ), the HYDROWEB database (H-W, date in parentheses), and the difference between them (ΔH-W–in situ).

Year	Water Level, m			Water Area, km^2			Water Volume, km^3		
	In Situ	H-W	$\Delta_{\text{H-W–in situ}}$, m	In Situ	H-W	$\Delta_{\text{H-W–in situ}}$, m^2	In Situ	H-W	$\Delta_{\text{H-W–in situ}}$, m^3
1999	1896.63	1897.87 (25.02)	+1.24	1239.71	1237.24 (25.02)	−2.47	33.30	33.16 (25.02)	−0.14
2001	1896.46	1897.83 (22.02)	+1.37	1237.89	1236.99 (22.02)	−0.9	33.09	33.11 (22.02)	+0.02
2007	1898.25	1899.84 (18.03)	+1.59	1255.96	1249.52 (18.03)	−6.44	35.33	35.61 (18.03)	+0.28

It can be seen that in 1995–2010 (at the stage of lowering the level and its subsequent increase), the altimetric values of the level exceeded those according to gauging stations in most cases by 1.1–1.5 m. This can partly be explained by the discrepancy between the dates for which the comparison was made, but even for the same dates in 1998 (Table 1), the difference in values was 1.13 m. From 2013 to 2022 (stage of small-level change), this difference was mainly within 0.6 m (Table 2). A comparison of the data from the Center for Hydrometeorology and Monitoring of Armenia [67] for June and November 2022 (1900.75 and 1900.37 m BS, respectively) with altimetric data (1901.23–1901.3 m and 1900.73–1900.79 m BS) gives the difference between the two types of data within 0.55 and 0.42 m, respectively; in May 2021, with the highest level in 2021–2022 equal to 1900.90 m BS, and altimeter data equal to 1901.33–1901.4 m BS, the difference was also within 0.5 m. Thus, it can be assumed that since 2013 (a period of relative level stabilization), altimetry level values have exceeded the available measured values at gauging stations by approximately 0.5–0.6 m.

The few available data allow us to compare simultaneously the level, surface area, and water volume obtained by field and satellite measurements at close dates (Table 3). Note that, as noted in Section 2.2, the HYDROWEB database does not contain the values of the lake's water volume, but its increments relative to the reference value as of 18 June 1995. In the literature, there are values of morphometric parameters only for 31 December 1995 [2]: level—1896.75 m BS, surface area—1238.8 km^2, water volume—33.20 km^3. The volume values for the dates indicated in Table 3 are given taking into account the increments relative to this reference value given in the HYDROWEB database, equal to −0.04 km^3 for 1999, −0.09 km^3 for 2001, and +2.41 km^3 for 2007. According to Table 3, in 1999, 2001, and 2007, higher values of the level of the HYDROWEB database compared to the data from gauging stations corresponded to smaller surface areas and smaller (in 1999), approximately equal (in 2001), or larger (in 2007) volume values. The same trend of a smaller surface area (in the HYDROWEB database) at a higher level is found when comparing the values of the surface area on 1 January 2017: according to the data of the Ministry of Emergency Situations of the Republic of Armenia, given in [8], the surface area of Lake Sevan was 1278.6 km^2 (the level is not indicated, but, in accordance with Table 2, it was equal to 1900.46 m), and according to the HYDROWEB database on the same day (at a level of 1901.03 m), it was 1256, 94 km^2.

Let us also compare the data on the lake level and its volume presented in [66] for July 2021 with the corresponding values in the HYDROWEB database. With a level mark of 1900.75 m BS and a volume of 38 km^3 in [66], the level values in the HYDROWEB database were in the range of 1901.44–1901.2 m BS (i.e., 0.69–0.45 m above that given in [66]), and the volume increment relative to the reference value (33.20 km^3) amounted to +(4.42–4.12) km^3. Thus, the volume values of 37.62–37.32 km^3 in the HYDROWEB database in July 2021 turned out to be 0.38–0.68 km^3 (i.e., 1–1.8%) lower than those given in the work [66].

4. Discussion

Remote sensing data with high spatial resolution has been successfully used in recent years to solve various problems directly or indirectly related to monitoring the ecological state of Lake Sevan. These are studies of the spatio-temporal dynamics of lake surface temperature [13], spatio-temporal variations of phytoplankton biomass [17,27,68], the dynamics of the coastline [7,14] and water surface area [7], and environmental monitoring of Lake Sevan's coastal zone with small unmanned aerial vehicles [8]. Our article (together with recent works by the authors [28,29]) is the first study of the variability of the eddy dynamics of the surface layer of Lake Sevan, based on the analysis of satellite information for the summer–autumn period of different years. This study is especially relevant in the modern period due to the need to control the ecological state of the eutrophicated Lake Sevan, since, on the one hand, it is the eddy structures (monopoles, dipoles, or mushroom-shaped currents, and their packings) that largely determine the horizontal distribution of various types of suspended matter (including phytoplankton) in the waters of various lakes and seas [33,46,49,50,54,62,64,69–73]; on the other hand, the organization of quasi-synchronous instrumental measurements on the scale of the entire lake with variable eddy dynamics in it is practically unrealistic.

From the point of view of geophysical hydrodynamics, depending on the ratio A of the baroclinic Rossby radius of deformation Rd to the characteristic horizontal size of the lake L, lakes are divided into large, medium, and small (A = 0.03–0.05, 0.1–0.3, and 0.3–0.5, respectively) [74]. Our assessment based on the results of the vertical distribution of water temperature in Large Sevan in the third ten days of July and the first ten days of October 2018 and 2019 [34] gave an Rd of $\approx$ 3 km, with the characteristic size of the deep-water part of Large Sevan L $\approx$ 30 km A $\approx$ 0.1. Consequently, Lake Sevan belongs to the medium-sized lakes in which the effect of the Earth's rotation, as in large lakes and the ocean, affects large-scale water circulation, which suggests a cyclonic circulation of water in this lake. Works of the 1970s–1980s on hydrodynamic modeling of currents in Lake Sevan, [35–38], as well as field measurements of the temperature field (density) and current measurements at a few automatic buoy stations [33,34], mainly also indicate the cyclonic movement of water in the deep-water basin of Large Sevan. However, our study shows that there is no constant cyclonic circulation of water here, and in most cases, there are intense eddy dynamics that change noticeably on a time scale of several days. It became possible to establish this fact only through the analysis of high-spatial-resolution satellite images. Previous analyses of hydrological data, current maps, and numerical modeling were unable to detect the existing intense eddy dynamics of the waters due to the low spatial resolution, which could only reveal the average cyclonic circulation in the lake.

4.1. Nonstationary Eddy Dynamics of the Waters of Large Sevan

As the analysis of satellite images (Figures 2–6) shows, eddies, eddy dipoles, and packings of eddy dipoles (mushroom-shaped flows) of different spatial scales occupy almost the entire Large Sevan. The sizes of eddy structures in the basin vary over a wide range—from approximately 3 to 20 km, i.e., taking into account our estimated value of the baroclinic Rossby radius of deformation (approximately 3 km), both mesoscale and submesoscale eddies are observed (the eddy radius is greater than or less than Rd, respectively) [62,64,71,75–77].

A permanent element of the horizontal circulation of the deep-water part of Large Sevan is the cyclonic eddy, but its size varies in different situations from approximately 9–12 km in the central part of the basin (Figures 3f and 5a) to the scale of the entire deep-water part of the basin (Figure 4c–e). The situation, when the cyclonic circulation covers almost the entire deep-water basin, is rarely observed (Figure 4c–e). Most often, a cyclonic eddy forms dipoles or multipoles with anticyclones having a smaller diameter (for example, with attached anticyclones on its periphery, as in Figure 3b,d, or with dipoles in the eastern part of the basin, as in Figures 4h,j,k, 5a,c,d and 6b) or comparable to it. Of particular interest is the two-cell horizontal circulation, which occupies almost the entire deep-water

basin when the dipole consists of a cyclone and an anticyclone of approximately equal size (Figures 3e, 4a,g,j, 5c,d and 6c). In some images, it is a dipole with a horizontal axis between oppositely polar eddies, oriented to the west (Figures 3e, 4a,g and 5c). In other images, the dipole axis is tilted at approximately 45–60 degrees, pointing southwest (Figures 5d and 6c), or vertical, pointing south (Figure 4j). Moreover, when comparing Figure 5c,d, separated by a time interval of 5 days, it appears that the dipole with an inclined axis in Figure 5d could result from the rotation of the zonally oriented dipole in Figure 5c in the cyclonic (counterclockwise) direction. Note that the image in Figure 5c even suggests a three-cell circulation, with a smaller anticyclone between the cyclonic eddy and the southern coast of Large Sevan west of Cape Tsovinar. We can assume the presence of a tripole also in the dynamic situation shown in Figure 6c, where, in addition to the dipole in the central part of the basin, there is an anticyclonic eddy of smaller diameter in the eastern part of Large Sevan. In this case, the axis between eddies of the left dipole of the tripole structure is directed from northeast to southwest, and the right one is directed in the opposite direction.

The picture of two-cell circulation in the deep-water part of Large Sevan, shown in Figures 3e, 4a,g, 5c,d and 6c, are qualitatively similar to the horizontal circulation simulation results in southern Lake Michigan (USA). This is a two-cell circulation with a rotation of the dipole axis in the cyclonic direction over time at a constant wind direction (Figure 12 in [78]) (the scheme is also reproduced in two other works (Figure 2.20 in [33], Figure 11 in [79])), although the model circulation corresponds to a different morphometry of the lake—an elliptical shape of the basin and a parabolic bottom profile.

The time interval between successive optical satellite images of 5 days does not allow us to trace the formation and evolution of the two-cell circulation in the deep-water basin of Large Sevan. However, it is clear that the time scale of such horizontal circulation variability is less than five days. Note also that such circulation occurs in different months and different years: 11 July and 14 September 2019 (Figure 4a and Figure 4g, respectively), October 18 and 23 (Figure 5c and Figure 5d, respectively), and 3 September 2022 (Figure 6c). This fact, together with the time scale of the phenomenon, suggests that the determining factor in the formation of such a dipole structure on the scale of a deep-water basin is not the bottom topography/orography of the coast and not the features of thermal stratification (baroclinicity), but the intensity and direction of the wind effect. The direction of the horizontal axes of the dipoles in Figures 3e, 4a,g and 5c assumes an easterly wind. It is the eastern wind direction over Large Sevan that is predominant in the summer [12,31,80], although the prevailing wind directions in different areas of the lake are different and correspond mainly to the directions of the mountain ranges surrounding the lake basin (mountain valley winds) [5,6]. This is clearly visible in the radar images presented in this article and in [29], and additionally, the wind field can change noticeably on time scales of a day and, perhaps, smaller. It is likely that it is the impact of variable and multidirectional winds on the heated near-surface layer that determines such a variable (on time scales of several days or less) pattern of currents.

Recent studies of the horizontal circulation in Lake Sevan, carried out in the third ten days of July and the first ten days of October 2019 [34], make it possible to compare field data on the structure of currents in Large Sevan with satellite images of similar dates analyzed by us. In the third ten days of July 2019, according to field data (Figure 2b in [34]), a general cyclonic circulation was observed in Large Sevan on the scale of the deep-water basin. At the same time, the movement of floats with a sail in the area south of the Artanish Bay was directed to the northwest. This current structure is in good agreement with that recorded by the satellite on 31 July 2019 (Figure 4c). In the first ten days of October 2019, as noted by the authors of [34], "the area of the cyclonic gyre in Large Sevan was shifted to the western shore", and the floats south of the Artanish Bay moved south (Figure 2d in [34]). This current pattern also does not contradict the satellite image from 14 October 2019 (Figure 4k).

Satellite images also demonstrate a rarely observed feature of the internal structure of the cyclonic gyre in Large Sevan—the presence of two clearly interacting cyclonic eddies of

smaller diameter (Figure 4b,j). It should also be noted that the interaction of two cyclonic eddies located in different parts of the deep-water basin is sometimes observed. These are a cyclonic gyre in the southern part of Large Sevan and a smaller cyclone in the Artanish Bay connected by a jet stream (Figures 4h and 6b). We previously noted a similar connection by a jet stream of two eddies with the same direction of rotation for anticyclonic eddies in the northwestern part of the Black Sea (Figure 3 in [81]) and for cyclonic eddies in the southeastern Baltic Sea (Figure 1 in [62]). A cyclonic eddy (3–6 km in diameter) is the most commonly observed circulation element in the Artanish Bay (Figures 3f, 4c,h,k, 5c and 6b), sometimes an eddy dipole (Figure 4b).

A characteristic element of the horizontal circulation of water behind Cape Tsovinar is an anticyclonic eddy, comparable to the scale of the cape (Figures 2a, 3a,c, 4a and 6a,b), or a mushroom-shaped structure (Figures 3d,e, 4b,d and 5c,d). Eddy formation behind capes in lakes, seas, and the ocean is well known and is associated with the instability of the alongshore flow near inhomogeneities of the coastline [33,59,62,64,71,76,77,82]. In the shallow southeastern part of Large Sevan, the most often observed structures are not anticyclonic circulation, as follows from the modeling results [35], or the lake circulation diagram in [34], but eddy dipoles with an axis directed to the west (Figures 3b,c,f and 4a,c,h,g) or to the east (Figures 4h and 5c). In Figure 4h, two counter-directed eddy dipoles are seen, of which the one closest to the shore (eddy diameter of 2.5 km) is oriented to the west (this appears to be the mushroom-shaped flow of the Masrik River). An element of anticyclonic vorticity in the southeastern region, located east of the cyclonic gyre and forming a dipole structure with it, is visible in Figure 4b.

4.2. Eddy Dynamics of the Waters of Small Sevan and Their Role in Water Exchange through the Strait

The cyclonic gyre in Small Sevan with a diameter of ≈8–9 km almost constantly appears on optical and SAR images in the summer–autumn period, which is consistent with the known results of hydrodynamic modeling and field observations. Unlike the cyclonic gyre in Large Sevan, it retains its spatial position to the north of the strait. Interestingly, as seen in the radar images (Figures 2b, 4f,i, 5b and 6d), the northern boundary of the gyre often coincides with the southern boundary of the northeasterly wind flow, which appears to contribute to the formation of this cyclonic gyre. The northeastern and northern wind directions, according to the works of [12,31,80], are predominant in summer over Small Sevan. The cyclonic gyre in Small Sevan in the presented satellite images appeared from July 11 (Figure 3a) to the end of October (Figure 3g).

The evolution of the cyclonic gyre is accompanied by the formation of elements of anticyclonic vorticity on its periphery (Figures 2a,b, 3g, 5b, 6b and 7a,b). In addition to this quasi-stationary cyclonic gyre, smaller cyclonic eddies or eddy dipoles and their combinations are formed in the northern part of Small Sevan (Figures 2a, 3a, 4g and 6a,d), apparently related to local features of bottom topography and wind influence.

It is traditionally believed that the movement of water from Large Sevan to Small Sevan occurs, in accordance with the general cyclonic circulation of the lake waters, along the eastern shore of the strait, and from Small Sevan to Large Sevan along its western shore [5,12,35,38,83]. In [83], based on the results of instrumental measurements, it is noted that in the summer, in the surface layer, currents from Large Sevan to Small Sevan are most pronounced near the northern shore of the strait (they decrease to the south), and in the southern shallow part of the strait, stable currents are not observed. As follows from the distributions of phytoplankton in the above satellite images, the cyclonic gyre in Small Sevan and its attached anticyclones, as well as eddies in the northern part of Large Sevan, close to the strait, influence water exchange through the strait. Thus, water from the shallow part of the western shore of Large Sevan near the strait is drawn along the eastern periphery of the cyclonic gyre into Small Sevan (Figures 3b,g and 4a,d,h,j), as well as by a small cyclonic eddy in the strait near Cape Artanish (Figure 5c). And vice versa, the attached anticyclone on the southern part of the periphery of the cyclonic gyre in Small Sevan, which partially ends up in the strait, transfers water from Small Sevan to Large

Sevan (Figure 2a). Similarly, a small cyclonic eddy near the strait, which is an attached eddy structure of the anticyclonic component of the eddy dipole in the deep-water part of Large Sevan, draws water from Small Sevan to Large Sevan (Figure 4g,k).

4.3. Morphometric Parameters of Lake Sevan

Like any information obtained from satellite measurements, the values of morphometric parameters in the HYDROWEB database need to be validated based on in situ measurements. Our comparison of level values from the HYDROWEB database with available in situ data showed that the level values measured by the altimeter exceeded the gauging data in most cases by more than 1 m in 1995–2012 and by 0.5–0.6 m in 2013–2022. The values of the surface area and volume of the lake waters (volume values are determined by increments in the HYDROWEB database using the reference volume value for 1995 known from the publication [2]), on the contrary, turn out to be underestimated (at a higher level) relative to published in situ data. Investigation of the reasons for the identified inconsistencies is beyond the scope of this article.

5. Conclusions

In this article, we analyzed and interpreted satellite ocean color data (MSI Sentinel-2) images and near-date radar (Sentinel-1) images of Lake Sevan during the period of 2017–2022 in order to identify the mechanisms of horizontal mixing of its waters and to establish to what extent the scheme of cyclonic water circulation in Large Sevan, based on the results of a few field measurements and hydrodynamic modeling, corresponds to the real picture of currents in the surface layer of this basin in the summer–autumn period. A validation of the morphometric parameters of the lake (level, surface area, and water volume) contained in the HYDROWEB database, based on data from satellite altimetry, optical satellite imagery, and algorithms for processing this satellite information developed in the LEGOS laboratory (France) [52,53], was also carried out comparing them with available instrumental measurements.

We have established that a constant cyclonic gyre does not exist on the scale of the deep-water part of Large Sevan. A mesoscale cyclonic eddy with varying size ($\approx$9–20 km) and center position is a constant element of the circulation of the deep-water basin of Large Sevan, and at certain periods of time (for example, in the first half of August 2019), satellite images actually display a cyclonic gyre on a scale of the deep-water basin (approximately 20 km). However, in most cases, non-stationary eddy dynamics are observed in Large Sevan, including mesoscale and submesoscale eddies, eddy dipoles (mushroom-shaped flows), and their packings. Often the entire deep-water part of Large Sevan is occupied by a two-cell (dipole) or even three-cell (cyclonic eddy with two anticyclones of similar size) water circulation with horizontal (westward), inclined (southwest-oriented) or vertical (south-directed) axes between dipole eddies with different directions of rotation. The time scale of the observed variability is several days and possibly smaller (due to the periodicity of the appearance of informative optical satellite images of 5 days, it is not possible to trace the evolution of a particular flow structure). The observation of such variable water circulation in different months (i.e., with different density stratifications of water) in different years raises the assumption that the main reason for the non-stationary dynamics in Large Sevan with a fairly homogeneous bottom and a slight indentation of the shoreline is the variability of the wind effect on the surface of the lake. Note that although the eastern wind prevails over Large Sevan in the summer season, local mountain valley winds of different directions are observed here, which is confirmed by the SAR images used in the work.

Apparently, due to strong and multidirectional winds, radar images for studying the eddy dynamics of Large Sevan are generally less effective compared to optical ones, and the number of informative radar images is less than optical ones. However, the combination of these two types of remote sensing on close dates provides additional information about local water circulation. In addition, it is the radar images that show the general picture

of multidirectional mountain–valley wind flows over the lake, while measurements at hydrometeorological stations provide information about local wind speed and direction.

The most frequently observed element of water circulation in the shallow southeastern part of Large Sevan is an eddy dipole; behind Cape Tsovinar there is an anticyclonic eddy comparable to the scale of the cape; in the Artanish Bay, there is a cyclonic eddy or dipole.

Analysis of satellite images showed that the constantly existing cyclonic gyre north of the strait in Small Sevan (diameter approximately 8–9 km) and attached anticyclonic eddies in the southern part of its periphery, as well as cyclonic submesoscale vortices in the northern part of Large Sevan, close to the strait, affect water exchange between Small and Large Sevan in both directions. Moreover, the flow of water from Large Sevan into Small Sevan due to its involvement by the cyclonic gyre of Small Sevan or a small cyclonic eddy in the strait near the Artanish Peninsula occurs from the western shore of Large Sevan, i.e., across the strait.

It is obvious that with such variable eddy dynamics of water in Large Sevan, revealed by this study, a hydrological survey with pre-planned positions of hydrological stations or buoy placements can provide unreliable information about the current system in the basin, as well as an interpretation of the results of hydrological survey without analysis of close in-time satellite information. Modern hydrological studies of Lake Sevan should be carried out taking into account quasi-synchronous optical satellite information, ideally using satellite guidance to the research object.

Our analysis of satellite optical images showed that non-stationary mesoscale and submesoscale eddy circulation elements in Large and Small Sevan largely determine the spatiotemporal variability of phytoplankton distribution throughout the lake. Therefore, when taking phytoplankton samples, it is advisable to "link" as much as possible to quasi-synchronous satellite information and analyze the biological parameters of the samples taken taking this into account.

Such vortex processes regularly appear, for example, in the Gdansk Bay of the Baltic Sea, where they are recorded on optical images due to the bloom of cyanobacteria, as well as in Lake Sevan. The annual subsatellite measurements we carried out allowed us not only to validate radar and optical images for the presence of vortices but also to determine their three-dimensional structure [84]. Based on the experience of validating eddy processes in the Gdansk Bay, we can confidently say that the parameters of eddies in Lake Sevan, determined from optical images, correspond with great accuracy to the vortex pattern in the lake.

There are evident advantages to remote sensing methods in the investigation of mesoscale and submesoscale water dynamics in Lake Sevan, but there are also several disadvantages. First, to identify eddies on optical and infrared imagery we need any kind of contrast. Our analysis of these data for 2017–2022 has shown that this is possible only during summer months when high concentrations of chlorophyll (and its contrasts) are observed during algal blooms. Thermal imagery has a lower spatial resolution of 100 m, and in Lake Sevan, we did not find significant water temperature contrasts which could help to detect submesoscale eddies. Both optical and thermal methods are seriously restricted by cloudiness, which is often observed in this mountain region and which prevents the acquisition of informative (cloudy-free) imagery. SAR data on the roughness of the water surface, in many cases, are useless for vortex detection, because there are no films of surfactants (for example, as a result of phytoplankton blooms), which can damp the gravity–capillary waves on the water surface. Also, wind speed over Lake Sevan is often very low which is outside of the best range for the manifestation of eddy structures in radar images.

In addition, in radar images, vortex processes can manifest themselves not only due to the presence of a biogenic film on the surface but also due to the so-called shear-wave mechanism, due to the interaction of waves and currents in the region of the cyclonic current shear. In this case, the vortices appear as spirals or arcs of increased signal scattering [85]. This mechanism of manifestation of small-scale vortices does not make it possible to study their fine spatial structure; regions of increased brightness associated with divergent zones

usually "draw" only the outer contour of the vortex or vortex dipole. But this also provides additional information about the presence of eddies in a specific water area during strong winds, when biogenic films are destroyed, or in winter, during their absence. However, in winter, in the presence of unstable stratification, when the water is warmer than the air, which is typical for a non-freezing Lake Sevan (the lake freezes only in very severe winters), on radar images, all hydrodynamic processes are masked either by manifestations of convective processes in the surface layer of the atmosphere or by areas of increased brightness of the radar signal associated with strong winds.

Our validation of the morphometric parameters of Lake Sevan in the HYDROWEB database based on their comparison with the available instrumental measurement data showed that at higher level values in the HYDROWEB database relative to the gauging station data (by about 0.5–0.6 m in the modern period), the values of surface area and water volume turned out to be underestimated, which does not correspond to the known bathymetry of Lake Sevan. The reasons for this discrepancy require special research. However, already now time sequences of Lake Sevan level values in almost real time and with good time resolution (periodicity—no more than a month in recent years), available in the near-real time HYDROWEB database, can be a convenient tool for the monitoring of level changes in the modern period when the level can change both as a result of planned rises/decreases in the lake level and as a result of global and local climate changes.

References

1. Babayan, A.; Hakobyan, S.; Jenderedjian, K.; Muradyan, S.; Voskanov, M. Lake Sevan: Experience and Lessons Learned Brief. International Waters Learning Exchange & Resource Network. 2005, pp. 347–362. Available online: https://iwlearn.net/resolveuid/6af5017fa3a56bc7b8428f71c100362e (accessed on 19 March 2024).
2. *Integrated Assessment of the Ecological State of Lake Sevan (GEO–Lake Sevan)*; Association "For Sustainable Human Development"/UNEPCom: Yerevan, Armenia, 2011; 42p, Available online: https://gridarendal-website-live.s3.amazonaws.com/production/documents/:s_document/92/original/sevan-report---fin.pdf?1483646517 (accessed on 19 March 2024). (In Russian)
3. Wilkinson, I.P. Lake Sevan: Evolution, Biotic Variability and Ecological Degradation. In *Large Asian Lakes in a Changing World*; Mischke, S., Ed.; Springer Water; Springer: Cham, Switzerland, 2020; pp. 35–63. [CrossRef]
4. Arutyunyan, D.V.; Muradyan, M.A. Lake Sevan as the most important source of water resources of the Republic Armenia. *Reg. Probl. Econ. Transform.* **2021**, *6*, 127–134.
5. Oganesyan, R.O. *Lake Sevan Yesterday, Today*; Publishing House of NAS RA "Gitatyun": Yerevan, Armenia, 1994. (In Russian)
6. Rumyantsev, V.A.; Drabkova, V.G.; Izmailova, A.G. Lake Sevan. In *Great Lakes of the World*; Lema: St. Petersburg, Russia, 2012; pp. 271–280. (In Russian)
7. Matishov, G.G.; Selyutin, V.V.; Mestopyan, K.E.; Bulysheva, N.I.; Sheverdyaev, I.V.; Aroutiounian, N.M.; Gabrielyan, B.K. Current state and problems of the study of Lake Sevan. *Sci. South Russ.* **2016**, *12*, 43–52. (In Russian)

8. Medvedev, A.; Telnova, N.; Alekseenko, N.; Koshkarev, A.; Kuznetchenko, P.; Asmaryan, S.; Narykov, A. UAV-derived data application for environmental monitoring of the coastal area of Lake Sevan, Armenia with a changing water level. *Remote Sens.* **2020**, *12*, 3821. [CrossRef]

9. Why Sevan "Blooms" and How to Deal with It—The Ministry of the Environment Explained, SPUTNIK, Armenia, 31 July 2022. Available online: https://ru.armeniasputnik.am/20220730/pochemu-tsvetet-sevan-i-kak-s-etim-borotsya--minokruzhayuschey-sredy-poyasnilo-45912598.html (accessed on 19 March 2024). (In Russian)

10. Sarkisyan, L. Impact on the Sevan Ecosystem: The Dangers of Additional Water Intake, SPUTNIK, Armenia, 31 July 2023. Available online: https://ru.armeniasputnik.am/20230731/udar-po-ekosisteme-sevana-chem-opasen-dopolnitelnyy-zabor-vody-63628469.html (accessed on 19 March 2024). (In Russian)

11. Gozalyan, M.G. On the thermal regime of Lake Sevan in connection with the descent of its level. *Proc. Sevan Hydrobiol. Stn.* **1979**, *XVII*, 5–23. (In Russian)

12. Ecology of Lake Sevan during the period of water level rise. In *The results of Russian-Armenian Biological Expedition for Hydroecological Survey of Lake Sevan (Armenia) (2005–2009)*; Nauka, Dagestan Scientific Center: Makhachkala, Russia, 2010; ISBN 978-5-94434-162-4. (In Russian)

13. Hovsepyan, A.; Muradyan, V.; Tepanosyan, G.; Minasyan, L.; Asmaryan, S. Studying the dynamics of Lake Sevan water surface temperature using Landsat 8 satellite imagery. *Ann. Valahia Univ. Targoviste. Geogr. Ser.* **2018**, *18*, 68–73. [CrossRef]

14. Hovsepyan, A.; Tepanosyan, G.; Muradyan, V.; Shushanik, A.; Medvedev, A.; Koshkarev, A. Lake Sevan shoreline change assessment using multi-temporal Landsat images. *Geogr. Environ. Sustain.* **2019**, *12*, 212–229. [CrossRef]

15. Hovsepyan, A.A.; Gambaryan, L.R.; Mamyan, A.A. Some information about blue-green algal blooms in Lake Sevan. Lakes of Eurasia: Problems and Solutions. In Proceedings of the 1st International Conference 2017, Petrozavodsk, Russia, 11–15 September 2017; pp. 547–550. (In Russian)

16. Hovsepyan, A.A.; Mamyan, A.S.; Khachikyan, T.G.; Tikhonova, I.V.; Sorokovikova, E.G.; Belykh, O.I.; Gevorgyan, G.A. Monitoring of phytoplankton status in Lake Sevan (Armenia) in 2018. *Proc. Yerevan State Univ.* **2019**, *53*, 206–211. [CrossRef]

17. Gevorgyan, G.; Rinke, K.; Schultze, M.; Mamyan, A.; Kuzmin, A.; Belyakh, O.; Sorokovikova, E.; Hayrapetyan, A.; Hovsepyan, A.; Khachikyan, T.; et al. First report about toxic cyanobacterial bloom occurrence in Lake Sevan, Armenia. *Int. Rev. Hydrobiol.* **2020**, *105*, 131–142. [CrossRef]

18. Sakharova, E.G.; Krylov, A.V.; Sabitova, R.Z.; Tsvetkov, A.I.; Gambaryan, L.R.; Mamyan, A.S.; Gabrielyan, B.K.; Hayrapetyan, A.O.; Khachikyan, T.G. Horizontal and vertical distribution of phytoplankton in alpine Lake Sevan (Armenia) during the summer water blooms of Cyanoprokaryota. *Sib. Ecol. J.* **2020**, *1*, 76–88. (In Russian)

19. Avalyan, R.E.; Atoyants, A.L.; Hambaryan, L.R.; Aghajanyan, E.A.; Gabrielyan, B.K.; Aroutiounian, R.M. Assessment of the state of Lake Sevan water during the summer using model test-objects. *Trans. Papanin Inst. Biol. Inland Waters RAS* **2022**, *98*, 26–37. [CrossRef]

20. NASA's Earthobservatory, Image of the Day—2 May 2023. Available online: https://earthobservatory.nasa.gov/images/151363/algae-in-the-andes (accessed on 26 September 2023).

21. Nasrollahzadeh, H.; Makhlough, A.; Pourgholam, R.; Vahedi, F.; Qanqermeh, A.; Foong, S. The study of Nodularia spumigena bloom event in the Southern Caspian Sea. *Appl. Ecol. Environ. Res.* **2011**, *9*, 141–155. [CrossRef]

22. Medvedeva, A.V.; Stanichny, S.V.; Kubryakov, A.A. Intensive development of cyanobacteria in the southern part of the Caspian Sea. *Sovremennye Problemy Distantsionnogo Zondirovaniya Zemli iz Kosmosa* **2023**, *20*, 253–268. [CrossRef]

23. Lavrova, O.Y.; Mityagina, M.I.; Kostianoy, A.G. *Satellite Methods in the Study of the Caspian Sea Variability*; IKI RAN: Moscow, Russia, 2022. (In Russian)

24. Kahru, M.; Elmgren, R.; Kaiser, J.; Wastmund, N.; Savchuk, O. Cyanobacterial blooms in the Baltic Sea: Correlations with environmental factors. *Harmful Algae* **2020**, *92*, 101739. [CrossRef] [PubMed]

25. Aleskerova, A.A.; Kubryakov, A.A.; Stanichny, S.V.; Lishaev, P.N.; Mizyuk, A.I. Cyanobacteria bloom in the Azov Sea according to Landsat data. *Izv. Atmos. Ocean. Phys.* **2019**, *55*, 1416–1426. [CrossRef]

26. Kubryakov, A.A.; Lishaev, P.N.; Aleskerova, A.A.; Stanichny, S.V.; Medvedeva, A.A. Spatial distribution and interannual variability of cyanobacteria blooms on the North-Western shelf of the Black Sea in 1985–2019 from satellite data. *Harmful Algae* **2021**, *110*, 102–128. [CrossRef]

27. Asatryan, V.; Stepanyan, L.; Hovsepyan, A.; Krachikyan, T.; Mamyan, A.; Gambaryan, L. The dynamics of phytoplankton seasonal development and its horizontal distribution in Lake Sevan (Armenia). *Environ. Monit. Assess.* **2022**, *194*, 757. [CrossRef] [PubMed]

28. Ginzburg, A.I.; Kostianoy, A.G.; Sheremet, N.A.; Kouraev, A.V. Horizontal water circulation and morphometric parameters of Lake Sevan in the modern period (satellite information). *Sovrem. Probl. Distantsionnogo Zondirovaniya Zemli iz Kosmosa* **2023**, *20*, 230–243. [CrossRef]

29. Ginzburg, A.I.; Sheremet, N.A.; Kostianoy, A.G.; Lavrova, O.Y. On the horizontal water circulation in Lake Sevan (satellite information). *Sovrem. Probl. Distantsionnogo Zondirovaniya Zemli iz Kosmosa* **2023**, *20*, 258–275. [CrossRef]

30. Davydov, V.K. Thermals of Lake Sevan. In *Materials on the Investigation of Lake Sevan and Its Basin*; Gidrometizdat: Leningrad, Russia, 1934; Pt. II. (In Russian)

31. Ainbund, M.M. On the issue of the thermal regime of Lake Sevan. In *Results of Comprehensive Research on the Sevan Problem*; Armenian SSR: Yerevan, Armenia, 1961; pp. 323–335. (In Russian)

32. Bukin, V.M. Special postcards for collecting information about surface currents in water bodies. *Meteorol. Hydrol.* **1974**, *2*, 82–85. (In Russian)

33. Filatov, N.N. *Hydrodynamics of Lakes*; Nauka, St. Petersburg Branch: St. Petersburg. Russia, 1991. (In Russian)

34. Poddubnyi, S.A.; Gabrielyan, B.K.; Tsvetkov, A.I. The present-day structure of the temperature and current fields in Lake Sevan. *Water Resour.* **2023**, *50*, 787–793. [CrossRef]

35. Torgomyan, G.M. Currents of Lake Sevan. *Izv. Acad. Sci. Armen. SSR* **1975**, *XXIII*, 45–50. (In Russian)

36. Akopyan, M.A.; Torgomyan, G.M. Calculation of the velocity field of Lake Sevan by mathematical modeling. *Izv. Acad. Sci. Armen. SSR Ser. Tech. Sci.* **1980**, *XXXIII*, 34–39. (In Russian)

37. Akopyan, M.A.; Demin, Y.L. Numerical modeling of the currents of Lake Sevan. *Meteorol. Hydrol.* **1982**, *8*, 68–74. (In Russian)

38. Akopyan, M.A.; Gurina, A.M.; Demin, Y.L.; Filatov, N.N. Diagnostic model for calculating currents in stratified lakes. *Izv. All-Union Geogr. Soc.* **1984**, *116*, 28–32. (In Russian)

39. Kireev, I.A. Hydrographical Survey of the Lake Sevan. In *Materials on the Investigation of Lake Sevan and Its Basin*; Transcaucasian Sevan Committee: Leningrad, Russia, 1933; part V. (In Russian)

40. Emery, K.O.; Csanady, G.T. Surface circulation of lakes and nearly land-locked seas. *Proc. Nat. Acad. Sci. USA* **1973**, *70*, 93–97. [CrossRef]

41. Kosarev, A.N. *Hydrology of the Caspian and Aral Seas*; Moscow University: Moscow, Russia, 1975. (In Russian)

42. Izhitskiy, A.S.; Zavialov, P.O.; Roget, E.; Huang, H.-P.; Kurbaniyazov, A.K. On thermohaline structure and circulation of the Western Large Aral Sea from 2009 to 2011: Observations and modeling. *J. Mar. Syst.* **2014**, *129*, 234–247. [CrossRef]

43. Sutyrina, E.N. The study of vortex structures in Lake Baikal using remote sensing data. *Int. Res. J.* **2016**, *7*, 157–159. (In Russian)

44. McKinney, P.; Holt, B.; Matsumoto, K. Small eddies observed in Lake Superior using SAR and sea surface temperature data. *J. Great Lakes Res.* **2012**, *38*, 786–797. [CrossRef]

45. Kostianoy, A.G.; Soloviev, D.M.; Kostianaia, E.A.; Sirota, A.M. Satellite remote sensing of Lake Skadar/Shkodra. In *The Skadar/Shkodra Lake Environment*; Pesic, V., Karaman, G., Kostianoy, A.G., Eds.; Springer International Publishing AG: Cham, Switzerland, 2018; pp. 89–120. [CrossRef]

46. Hamze-Ziabari, S.M.; Foroughan, M.; Lemmin, U.; Barry, D.A. Monitoring mesoscale to submesoscale processes in large lakes with Sentinel-1 SAR imagery: The case of Lake Geneva. *Remote Sens.* **2022**, *14*, 4967. [CrossRef]

47. Kostianoy, A.G.; Lebedev, S.A.; Solovyov, D.M. Satellite monitoring of the Caspian Sea, Kara-Bogaz-Gol Bay, Sarykamysh and Altyn Asyr Lakes, and Amu Darya River. In *The Turkmen Lake Altyn Asyr and Water Resources in Turkmenistan*; Zonn, I.S., Kostianoy, A.G., Eds.; The Handbook of Environmental Chemistry Series; Springer: Berlin/Heidelberg, Germany, 2013; Volume 28, pp. 197–231. [CrossRef]

48. Ginzburg, A.I.; Kostianoy, A.G.; Sheremet, N.A. On the dynamics of waters in the Kara-Bogaz-Gol Bay (satellite information). *Sovrem. Probl. Distantsionnogo Zondirovaniya Zemli iz Kosmosa* **2022**, *19*, 265–279. [CrossRef]

49. Ginzburg, A.I.; Kostianoy, A.G.; Sheremet, N.A.; Soloviev, D.M. Vortices in the Western Large Aral Sea (satellite information). *Sovrem. Probl. Distantsionnogo Zondirovaniya Zemli iz Kosmosa* **2021**, *18*, 236–246. [CrossRef]

50. Ginzburg, A.I.; Kostianoy, A.G.; Sheremet, N.A.; Soloviov, D.M. On the question of vortex dynamics of waters in the western basin of the Aral Sea. *Sovrem. Probl. Distantsionnogo Zondirovaniya Zemli iz Kosmosa* **2022**, *19*, 106–114. [CrossRef]

51. NASA's Earthobservatory, Image of the Day—12 September 2016. Available online: https://earthobservatory.nasa.gov/images/92591/lake-van-turkey (accessed on 27 September 2023).

52. Cretaux, J.-F.; Arsen, A.; Calmant, S.; Kouraev, A.; Vuglinski, V.; Berge-Nguyen, M.; Gennero, M.-C.; Nino, F.; Abarca Del Rio, R.; Cazenave, A.; et al. SOLS: A lake database to monitor in the near real time water level and storage variations from remote sensing data. *Adv. Space Res.* **2011**, *47*, 1497–1507. [CrossRef]

53. Cretaux, J.-F.; Nielsen, K.; Frappart, F.; Papa, F.; Calmant, S.; Benveniste, J. Hydrological applications of satellite altimetry: Rivers, lakes, man-made reservoirs, inundated areas. In *Satellite Altimetry over Oceans and Land Surfaces*; CRC Press: Boca Raton, FL, USA, 2017; pp. 459–504. [CrossRef]

54. Lavrova, O.Y.; Kostianoy, A.G.; Lebedev, S.A.; Mityagina, M.I.; Ginzburg, A.I.; Sheremet, N.A. *Complex Satellite Monitoring of the Russian Seas*; IKI RAN: Moscow, Russia, 2011. (In Russian)

55. Lavrova, O.Y.; Mityagina, M.I.; Kostianoy, A.G. *Satellite Methods of Detection and Monitoring of Marine Zones of Ecological Risks*; IKI RAN: Moscow, Russia, 2016. (In Russian)

56. Kostianoy, A.G.; Lavrova, O.Y.; Strochkov, A.Y. Satellite Instrumentation and Technique for Monitoring of Seawater Quality. In *Instrumentation and Measurement Technologies for Water Cycle Management*; Di Mauro, A., Scozzari, A., Soldovieri, F., Eds.; Springer Water; Springer: Cham, Switzerland, 2022. [CrossRef]

57. Dokken, S.T.; Wahl, T. Observations of Spiral Eddies along the Norwegian Coast in ERS SAR Images. FFI Rapport 96/01463. 1996.

58. Alpers, W.; Huhnerfuss, H. The damping of the ocean waves by surface films: A new look at an old problem. *J. Geophys. Res. Ocean.* **1989**, *94*, 625–626. [CrossRef]

59. Ivanov, A.Y.; Ginzburg, A.I. Oceanic eddies in synthetic aperture radar images. *J. Earth Syst. Sci.* **2002**, *111*, 281–295. [CrossRef]

60. Gurova, E.S.; Ivanov, A.Y. Appearance of sea surface signatures and current features in the South-Eastern Baltic Sea on the MODIS and SAR images. *Earth Res. Space (Issledovanie Zemli iz kosmosa)* **2011**, *4*, 41–54. (In Russian)

61. Gade, M.; Byfield, V.; Ermakov, S.; Lavrova, O.; Mitnik, L. Slicks as indicators for marine processes. *Oceanography* **2013**, *26*, 138–149. [CrossRef]

62. Ginzburg, A.I.; Bulycheva, E.V.; Kostianoy, A.G.; Solovyov, D.M. Vortex dynamics in the southeastern Baltic Sea from satellite radar data. *Oceanology* **2015**, *55*, 805–813. [CrossRef]

63. Lavrova, O.Y.; Mityagina, M.I. Manifestation specifics of hydrodynamic processes in satellite images of intense phytoplankton bloom areas. *Izv. Atmos. Ocean. Phys.* **2016**, *52*, 974–987. [CrossRef]

64. Kostianoy, A.G.; Ginzburg, A.I.; Lavrova, O.Y.; Mityagina, M.I. Satellite remote sensing of submesoscale eddies in the Russian Seas. In *The Ocean in Motion*; Velarde, M., Tarakanov, R., Marchenko, A., Eds.; Springer Oceanography; Springer: Cham, Switzerland, 2018; pp. 397–413. [CrossRef]

65. Vanhellemont, Q. Sensitivity analysis of the dark spectrum fitting atmospheric correction for metre- and decametre-scale satellite imagery using autonomous hyperspectral radiometry. *Opt. Express* **2020**, *28*, 29948–29965. [CrossRef]

66. Nazaretyan, H. The Ups and Downs of Lake Sevan. EVN Report. 26 July 2021. Available online: https://evnreport.com/magazine-issues/the-ups-and-downs-of-lake-sevan/ (accessed on 19 March 2024).

67. How the Level of Lake Sevan Has Changed over the Past Two Years. SPUTNIK, Armenia. 8 November 2022. Available online: https://ru.armeniasputnik.am/20221108/kak-menyalsya-uroven-ozera-sevan-za-poslednie-dva-goda-51011551.html (accessed on 19 March 2024). (In Russian)

68. Teponasayn, G.; Muradyan, V.; Hovsepyan, A.; Minasyan, L.; Asmaryan, S. A Landsat 8 OLI satellite data-based assessment of spatio-temporal variations of Lake Sevan phytoplankton biomass. *Ann. Valahia Univ. Targoviste Geogr. Ser.* **2017**, *17*, 83–89. [CrossRef]

69. Fedorov, K.N.; Ginsburg, A.I. "Mushroom-like" currents (vortex dipoles) in the ocean and in a laboratory tank. *Ann. Geophys.* **1986**, *4*, 507–516.

70. Ginzburg, A.I. Horizontal exchange processes in the near-surface layer of the Black Sea. *Earth Obs. Remote Sens.* **1994**, *12*, 190–202.

71. Zatsepin, A.G.; Kremenetskiy, V.V.; Ostrovskii, A.G.; Baranov, V.I.; Kondrashov, A.A.; Korzh, A.O.; Soloviev, D.M. Submesoscale eddies at the Caucasus Black Sea shelf and the mechanisms of their generation. *Oceanology* **2011**, *51*, 554–567. [CrossRef]

72. Kubryakov, A.; Plotnikov, E.; Stanichny, S. Reconstructing large- and mesoscale dynamics in the Black Sea region from satellite imagery and altimetry data—A comparison of two methods. *Remote Sens.* **2018**, *10*, 239. [CrossRef]

73. Kubryakov, A.; Aleskerova, A.; Plotnikov, E.; Mizyuk, A.; Medvedeva, A.; Stanichny, S. Accumulation and cross-shelf transport of coastal water by submesoscale cyclones in the Black Sea. *Remote Sens.* **2023**, *15*, 4386. [CrossRef]

74. Filatov, N.N.; Menshutkin, V.V. Problems of estimation of influence climate and antropogenic factors on to gydrothermodynamics and ecosystems of large stratified inland water bodies. *Sci. Notes RGGMU* **2017**, *48*, 120–147. (In Russian)

75. Karimova, S.S. Statistical analysis of submesoscale eddies in the Baltic, Black and Caspian seas using satellite SAR images. *Earth Res. Space (Issledovanie Zemli iz kosmosa)* **2012**, *3*, 31–47. (In Russian)

76. Zatsepin, A.; Kubryakov, A.; Aleskerova, A.; Elkin, D.; Kukleva, O. Physical mechanisms of submesoscale eddies generation: Evidences from laboratory modeling and satellite data in the Black Sea. *Ocean Dyn.* **2019**, *69*, 253–266. [CrossRef]

77. Aleskerova, A.; Kubryakov, A.; Stanichny, S.; Medvedeva, A.; Plotnikov, E.; Mizyuk, A.; Verzhevskaia, L. Characteristic of topographic submesoscale eddies off the Crimea coast from high-resolution satellite optical measurements. *Ocean Dyn.* **2021**, *71*, 655–677. [CrossRef]

78. Saylor, J.H.; Huang, J.C.K.; Reid, R.O. Vortex modes in Southern Lake Michigan. *J. Phys. Oceanogr.* **1980**, *10*, 1814–1823. [CrossRef]

79. Boyce, F.M.; Donelan, M.A.; Hamblin, P.F.; Murthy, C.R.; Simons, T.J. Thermal structure and circulation in the great lakes. *Atmos.-Ocean* **1989**, *27*, 607–642. [CrossRef]

80. Timofeev, M.P. *Meteorological Regime of Lake Sevan*; Hydrometeorological Publishing House: Leningrad, Russia, 1960. (In Russian)

81. Ginzburg, A.I.; Kostianoy, A.G.; Nezlin, N.P.; Soloviev, D.M.; Stanichny, S.V. Anticyclonic eddies in the northwestern Black Sea. *J. Mar. Syst.* **2002**, *32*, 91–106. [CrossRef]

82. Alpers, W.; Brandt, P.; Lazar, A.; Dagorne, D.; Sow, B.; Faye, S.; Hansen, M.W.; Rubino, A.; Poulain, P.-M.; Brehmer, P. A Small-scale oceanic eddy off the coast of West Africa studied by multi-sensor satellite and surface drifter data. *Remote Sens. Environ.* **2013**, *129*, 132–143. [CrossRef]

83. Ainbund, M.M. On the peculiarities of the thermal regime in the strait between Small and Big Sevan. *Izv. Acad. Sci. Armen. SSR* **1964**, *27*, 19–33. (In Russian)

84. Krayushkin, E.V.; Lavrova, O.Y.; Nazirova, K.R.; Elizarov, D.A. Three-dimensional structure and dynamics of coastal eddy dipoles in the Southeastern Baltic Sea: Results of remote sensing and oceanographic experiments in summer 2021. *Cosm. Res.* **2023**, *61* (Suppl. S1), S130–S140. [CrossRef]

85. Johannessen, J.; Kudryavtsev, V.; Akimov, D.; Eldevik, T.; Winther, N.; Chapron, B. On radar imaging of current features: 2. Mesoscale eddy and current front detection. *J. Geophys. Res. Ocean.* **2005**, *110*, C07017. [CrossRef]